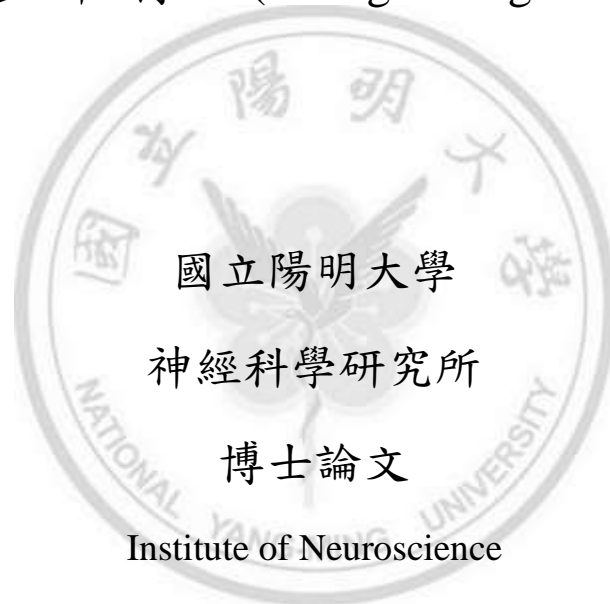


酸敏感離子通道在小鼠杏仁核網路的表現模式、特性與角色
Expression Pattern, Properties and Roles of Acid-Sensing Ion
Channels in the Mouse Amygdala Networks

研究生：江柏翰 (Po-Han Chiang)

指導教授：連正章 博士 (Cheng-Chang Lien, M.D., Ph.D.)



國立陽明大學

神經科學研究所

博士論文

Institute of Neuroscience

National Yang-Ming University

Doctoral Dissertation

中華民國一〇四年六月

June 2015

誌謝

感謝在這些年陪伴我、支持我、教導我的每一個人，讓我終於取得完成博士論文並且取得博士學位。自民國九十四年進入國立陽明大學生命科學系，到今年民國一百零四年取得博士學位，我在陽明待了整整十年，終於要離開陽明，非常開心，也有些感傷。從大學時期進入連正章老師的實驗室一直到取得博士學位，在不知不覺當中也已經過了七年，非常感謝連正章教授耐心的教導，讓我從一個懵懂無知、衝動魯莽的大學生，慢慢的磨成一個科學家、一個博士。連老師在科學上的實驗技術、實驗設計、還有文章撰寫；在做人處事與學習上的努力、與認真態度，都讓我受益良多。希望未來可以成為像連老師一樣成功的科學家。另外也要感謝大學時期的啟蒙老師—生命科學院范明基院長，當年的生命科學系系主任。大學二年級時，不但讓我在他的實驗室學習實驗方法，也在我成立陽明大學童軍社時幫了不少忙。雖然最後童軍社沒有成功，但就像之後許多實驗一樣，或許有些結果不如預期，但這都只是邁向目標的方法與過程，換個方法繼續努力，總會有成功的時候。

還要感謝葉韋均學長，在我進入實驗室的頭幾年教了我非常多電生理的知識與技術，帶領我慢慢了解神經電生理的世界，葉學長在畢業之後不久便過世了，希望他一路好走。另外，感謝實驗室所有一起努力的夥伴：翁儒韻、林晏竹、詹筑方、吳僕射、李政達、朱國彰、廖健璋、謝育鳴、黃昱尹、簡大鈞、陳建錚、許燦庭、郭寧、郭子維、許至緯、陳韋均、劉于超、高永恬、陳亭仔、侯文賢、顏廷耘、陳玠汝、林昱伶、高敏華、Ravi Chandra、王凱誼、紀廷璇、劉雅淇、郭翊慧、王思懿、鐘妮均、洪明欣、曹茵綢、謝瑀、陳勤霖、沈宏璋等人，在實驗遇到瓶頸時可以一起嬉戲歡笑，讓我可以撐過許多苦悶時光。

最重要的，我要感謝我的父親江豐文與母親王淑霞長年的養育與支持，讓我這些年可以無後顧之憂的取得博士，繼續的編織我的科學夢。還有哥哥江柏勳，雖然是電機領域，也時常與我分享一些有趣的想法，讓我可以學習跨領域的思考。最後，我最感謝最近才娶進門的老婆黃滄暉醫師。從大學二年即開始交往到現在，滄暉是我這些年最重要的精神支柱，沒有他的支持我絕對無法撐到現在，希望未來可以給滄暉更多的幸福，不負他的期望。

江柏翰

民國一〇四年六月十二日

Abstract

The amygdala is a complex structure involved in a wide range of normal behavioral functions and psychiatric conditions. Genetic variants in ACCN2, the human ortholog of acid-sensing ion channel-1a subunit (ASIC1a) gene, are associated with both panic disorder and amygdala structure and function. Animal studies showed that disrupting ASIC1a in mice reduces conditioned fear, which can be restored through transgenic expression of ASIC1a in the amygdala. Moreover, activity-induced long-term potentiation (LTP) of cortico-basolateral amygdala (BLA) synapses are impaired in ASIC1a-null mice, suggesting a critical role of ASICs in fear memory formation. Despite the importance of ASICs in fear-related behavior, very little is known about their expression pattern and properties in amygdala networks. Furthermore, the contribution of ASICs to synaptic plasticity in different cell types and synapses remains unknown. In this study, we have characterized the expression of ASICs in most amygdala cell types and LTP induction at multiple glutamatergic synapses in the amygdala network and found that the extent of LTP at various glutamatergic synapses correlated with the level of ASIC expression in postsynaptic neurons. More importantly, selective deletion of ASIC1a in GABAergic cells, including amygdala output neurons, eliminated LTP in these cells and reduced fear learning to the same extent as that found

when ASIC1a was selectively abolished in BLA glutamatergic neurons. Thus, these results indicate that fear learning requires ASIC-dependent LTP at multiple amygdala synapses, including both cortico-BLA input synapses as well as intra-amygdala synapses on output neurons.



中文摘要

杏仁核這個複合的結構參與在很多的正常行為與精神疾病。人類的酸敏感離子通道 1a 型的同源基因 ACCN2 的遺傳變異與恐慌症和杏仁核結構與功能有關聯。動物實驗也顯示，在小鼠剔除酸敏感離子通道 1a 型會降低制約的恐懼，這個現象可以經由轉基因表現酸敏感離子通道 1a 型在杏仁核而恢復。再者，酸敏感離子通道剔除鼠中，大腦皮質至側基核突觸的長期增益效應有缺陷，暗示著酸敏感離子通道在恐懼記憶形成中有關鍵作用。除了酸敏感離子通道在恐懼相關行為的重要性以外，對於其在杏仁核迴路中的表現模式與特性的了解非常的稀少。此外，酸敏感離子通道在不同細胞種類中突觸可塑性的貢獻也不清楚。在本研究中，我們測量了酸敏感離子通道在絕大多數杏仁核細胞種類的表現，及其對杏仁核迴路中多種麩胺酸性突觸長期增益效應的影響。發現長期增益效應在不同麩胺酸性突觸中的改變幅度與酸敏感離子通道在突觸後細胞的表現程度有正相關。更重要的是，選擇性在伽馬氨基丁酸性神經元中剔除酸敏感離子通道 1a 型（包含杏仁核往外輸出訊息的神經元）可以消除這些細胞的長期增益效應並且降低恐懼學習，且降低至與選擇性在側基核麩胺酸性神經元中剔除酸敏感離子通道 1a 型的小鼠一樣的程度。總而言之，這些研究結果指出，恐懼學習需要在多種杏仁核突觸中的酸敏感離子通道相依的長期增益效應，包含皮質輸入至側基核的突觸與杏仁核內傳至輸出訊息的神經元的突觸。

Table of Contents

誌謝	I
Abstract	II
中文摘要	IV
Table of Contents	V
Abbreviations	VIII

Chapter 1 Background and Specific Aims	1
1. Acid-sensing ion channels (ASICs)	1
1a. Structure of ASICs	1
1b. Characteristic of ASICs	2
1c. Location of ASIC subunits in the nervous system	3
1d. Distribution of ASICs in the brain	5
1e. Gating properties of ASICs in the brain	7
1f. Physiological function of ASICs in the brain	8
1g. ASICs in fear-related behaviors	10
1h. ASIC and diseases	11
2. Amygdala Network	13
2a. Center of fear learning and memory	13
2b. Basolateral amygdala (BLA)	15
2c. Central amygdala (CeA)	17
2d. Intercalated cell masses (ICMs)	18
2e. Fear learning circuitry	19
3. Specific aims	21
3a. Aim 1: Functional expression and properties of ASICs in amygdala.	21
3b. Aim 2: Functional role of ASICs in multiple glutamatergic synapses.	22
3c. Aim 3: The contribution of ASICs in different cell types to fear behavior.	22

Chapter 2 Functional Expression and Roles of ASICs in Amygdala Network	24
Introduction	24
Materials and Methods	27
Brain slice preparation	27
Nucleated patch recordings	28
Immunohistochemistry	30
Hierarchical clustering analysis	31
Measurement of synaptic responses and LTP induction	32

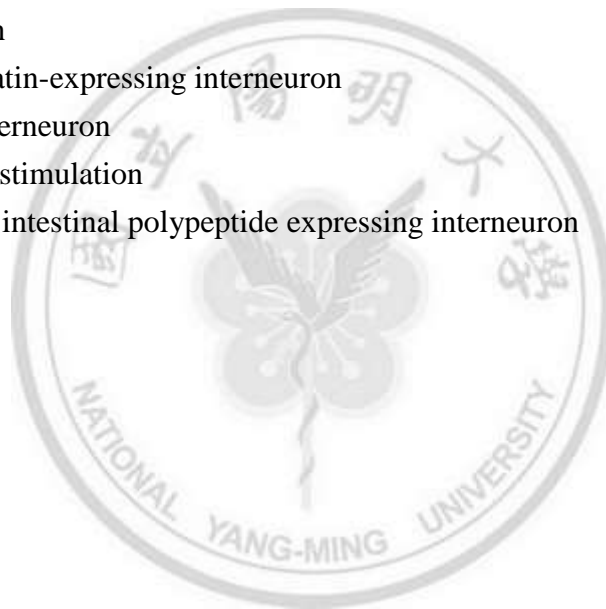
Fear conditioning -----	33
Virus injections -----	34
Data analysis and statistics -----	35
Results -----	38
GABAergic neurons are identified by GAD67-eGFP knock-in mice -----	38
Cell type-specific expression of ASICs in the BLA -----	39
Cell type- and subregion-specific ASIC expression in the CeA -----	42
Modest expression of ASIC in ICMs -----	43
ASICs in different types of amygdala neurons are functionally similar -----	44
Differential expression of ASICs selectively contributed to LTP in amygdala circuits -----	45
ASIC1a deletion in GABAergic neurons selectively impaired LTP at BLA-CeM neuron synapses -----	48
Deleting ASIC1a in BLA-PNs impaired conditioned fear learning -----	49
Deleting ASIC1a in GABAergic neurons impaired conditioned fear learning ---	51
Conclusion -----	53
<hr/>	
Chapter 3 Discussion -----	54
Significance of this study -----	54
ASIC1a, 2a and 2b are coexpressed in amygdala neurons-----	55
ASIC is important in primary input and output station of amygdala circuitry ---	56
Postsynaptic ASIC is a positive regulator of synaptic plasticity -----	57
ASIC-dependent LTP at multiple glutamatergic synapse are required for fear conditioning-----	59
ASICs in subcellular level -----	59
The possible role of ASICs in the BLA-INs -----	61
The possible role of ASICs in fear extinction -----	63
ASICs may have different role in the amygdala during seizure -----	64
Functional role of CeM neurons -----	65
<hr/>	
Figures and Tables -----	68
Figures -----	68
Figure 1 Fear circuitry within the amygdala -----	68
Figure 2 GAD67-eGFP labeled cells in the amygdala complex -----	70
Figure 3 ASIC currents in mouse amygdala neurons -----	72
Figure 4 ASIC currents in mouse amygdala neurons were mediated by ASIC1a and ASIC2 subunits -----	74
Figure 5 Classification of GABAergic INs in the BLA -----	76

Figure 6 Mapping of ASIC expression in different types of BLA neurons ---	78
Figure 7 Classification of GABAergic neurons in the CeL -----	80
Figure 8 Two distinct major cell types in the CeM -----	82
Figure 9 Mapping of ASIC expression in major cell types of CeA -----	83
Figure 10 Mapping of ASIC expression in ICMs -----	84
Figure 11 Expression pattern of ASIC in the amygdala -----	85
Figure 12 ASIC current kinetics of different amygdala neurons -----	86
Figure 13 ASICs selectively contributed to LTP at glutamatergic synapses onto amygdala neurons -----	89
Figure 14 ASIC1a deletion in GABAergic neurons impaired LTP at CeM-LTB neuron synapses -----	91
Figure 15 Pan-neuronal deletion of ASIC1a impaired conditioned fear behavior -----	93
Figure 16 Selectively deletion ASIC1a in BLA-PNs impaired conditioned fear behavior -----	95
Figure 17 Deleting ASIC1a in GABAergic neurons impaired conditioned fear behavior -----	97
Tables -----	98
Table 1 Electrophysiological properties of neurons in the BLA -----	98
Table 2 Electrophysiological properties of the major cell types in the CeL ----	100
Table 3 Electrophysiological properties of the major cell types in the CeM ---	101
Table 4 Electrophysiological properties of neurons in the ICMs -----	102
<hr/>	
References -----	103
<hr/>	
Curriculum Vitae -----	116

Abbreviations

AAV, adeno-associated virus
AcIN, accommodating interneuron
AMPA, α -Amino-3-hydroxy-5-methyl-4-isoxazolepropionic acid
AP, action potential
ASIC, acid-sensing ion channels
BA, basal amygdala
BASIC, bile acid-sensitive ion channel
BLA, basolateral amygdala
BLINaC, brain, liver, intestinal Na⁺ channel
CaMKII, Ca²⁺/calmodulin-dependent protein kinases II
CCKIN, cholecystokinin-expressing interneuron
CeA, central amygdala
CeL, lateral part of central amygdala
CeM, medial part of central amygdala
CNS, central nervous system
CS, conditional stimulation
CV, coefficient of variation
DEG/ENaC, degenerin/epithelial Na⁺ channel
DFIN, delay-firing interneuron
DRG, dorsal root ganglion
ES, early-spiking
FSIN, fast-spiking interneuron
GAD, glutamic acid decarboxylase
GFP, green fluorescent protein
HFS, high-frequency stimulation
ICM, intercalated cell mass
ICM_L, lateral intercalated cell mass
ICM_{MD}, medial–dorsal intercalated cell mass
ICM_{MV}, medial–ventral intercalated cell mass
IN, interneuron
ISI, inter-spike interval
LA, lateral amygdala
IPB, lateral parabrachial nucleus
LS, late-spiking
LTB, low-threshold bursting

LTP, long-term potentiation
NMDA, *N*-methyl-D-aspartic acid
NR2B, *N*-methyl-D-aspartic acid receptor subtype 2B
O-LM, oriens lacunosum-moleculare
PcTX1, paslmotoxin 1
PKC- δ , protein kinase C- δ
PN, principal neuron
PNS, peripheral nervous system
PSD-95, postsynaptic density protein 95
PVIN, parvalbumin-expressing interneuron
 R_{in} , input resistance
RMP, resting membrane potential
s.e.m., standard error of mean
SOM, somatostatin
SOMIN, somatostatin-expressing interneuron
StIN, stuttering interneuron
US, unconditional stimulation
VIPIN, vasoactive intestinal polypeptide expressing interneuron
WT, wild-type
 τ , time constants



Chapter 1

Background and Specific Aims

1. *Acid-sensing ion channels (ASICs)*

1a. *Structure of ASICs*

First observation of acid-induced currents was in cultured spinal neurons in 1980s (Krishtal and Pidoplichko et al., 1980). Almost twenty years after the discovery, acid-sensing ion channels (ASICs) were first cloned and identified by Waldmann and colleagues. (Waldmann et al., 1997). ASIC is a proton-gated sodium channel which belongs to the Degenerin/Epithelial Na⁺ channel (DEG/ENaC) superfamily (Kellenberger and Schild, 2002). To date, eight isoforms of ASIC subunit (ASIC1a, 1b, 1b2, 2a, 2b, 3, 4 and 5), which are produced by alternative splicing from five genes (ASIC1-ASIC5), have been identified (Ugawa et al., 2001; Lingueglia et al., 2007; Bioko et al., 2014). The crystal structure of the chicken ASIC1 deletion mutant shows that each subunit has two transmembrane domains with a large cysteine-rich

extracellular domain and small intracellular carboxyl and amino termini (Jasti et al., 2007). A functional ASIC is homo- or heterotrimeric structure formed by three subunits (Jasti et al., 2007). A recent study reports that ASIC1a and ASIC2a can randomly assemble heterotrimeric structure in both 1:2 and 2:1 compositions, which suggests that the heterotrimeric ASICs have flexible subunit stoichiometry. (Bartoi et al., 2014).

1b. Characteristic of ASICs

As a proton-gated Na⁺ channel, activation of ASIC by extracellular acidosis can cause a fast-rising and obvious desensitizing inward current (Waldmann et al., 1997). ASICs are preferentially permeable to Na⁺, but homotrimeric ASIC1a and heterotrimeric ASIC1a/2b channels are also have permeability to Ca²⁺ (Waldmann et al., 1997; Yermolaieva et al., 2004; Zha et al., 2006; Sherwood et al., 2011). In addition to protons, the large cysteine-rich extracellular domain of ASICs can also sense several modulators (Wemmie et al., 2013). All type of ASICs can be blocked by amiloride, a non-selective antagonist of degenerin/epithelial Na⁺ family. But only several specific subunits can be inhibited by peptides extracted from various animal venoms (Wemmie et al., 2013). For example, only ASIC1a homotrimer and ASIC1a/2b heterotrimer can be blocked by paslmotoxin 1 (PcTX1), a spider toxin extracted from the venom of the

South American tarantula *Psalmopoeus cambridgei*, through increasing its apparent proton affinity and trapping the channels in a inactivated state (Chen et al., 2005; Ziemann et al., 2009; Sherwood et al., 2011). Moreover, only ASIC3 homotrimer and ASIC3 containing heterotrimers can be blocked by APETx2, a sea anemone toxin isolated from *Anthopleura elegantissima* (Diochot et al., 2004). Finally, mambaglin, a snake toxin extracted from black mamba venom, can selectively block homotrimeric or heterotrimeric ASIC1a, ASIC1b, ASIC1a/1b, ASIC1a/2a, and ASIC1a/2b by binding the channels in a closed conformation (Diochot et al., 2012). Collectively, a transient inward current with obvious desensitization which can be induced by extracellular pH value drop, deep pH dependency, and Na⁺ selectivity are the hallmarks of ASICs.

1c. Location of ASIC subunits in the nervous system

A number of studies investigated the major members of ASIC family, including ASIC1a, 1b, 2a, 2b, and 3, in the nervous system in past few decades. Immunostaining, Western blotting and in situ hybridization results indicate that ASIC1a, 2a, and 2b have widespread distribution in the central nervous system (CNS) (Waldmann et al., 1997; Baron et al., 2002; Alvarez de la Rosa et al., 2003; Price et al., 2014). Whereas most subunits are expressed in the peripheral nervous system (PNS), including ASIC1a, 1b,

2a, 2b, and 3 (Wemmie et al., 2013; Lin et al., 2015). Among them, ASIC1b and ASIC3 are almost exclusively expressed in the PNS (Deval and Lingueglia, 2015). In the brain, ASICs are involved in the learning and memory processing in various brain regions (Wemmie et al., 2002; Du et al., 2014; Kreple et al., 2014), and play roles in a number of neurological diseases, for example, panic disorder, epilepsy, and ischemia (Smoller et al., 2014; Gao et al., 2005; Biagini et al., 2001). A recent study also shows that ASIC1a in the nucleus accumbens is important for drug addiction (Kreple et al., 2014). In the PNS, ASICs are involved in the mechanosensation, chemosensation and nociception (Baron et al., 2008; Lin et al., 2015; Deval and Lingueglia, 2015). Although numbers of studies indicate that the major members of ASICs are involved in many physiological function and neurological diseases, the underlying mechanism is not very clear.

Unlike the major subunits, the knowledge of role of ASIC1b2, ASIC4 and ASIC5 in the nervous system is poorly understood. ASIC1b2 is expressed in the trigeminal ganglion and dorsal root ganglion (DRG) (Ugawa et al., 2001). Unlike ASIC1b, acid-induced current cannot be detected in the homotrimeric ASIC1b2 in the transgenic *Xenopus* oocytes (Ugawa et al., 2001). ASIC4 is abundant in the pituitary gland and also expressed in several brain regions (Lin et al., 2015). ASIC5, which was called brain,

liver, intestinal Na⁺ channel (BLINaC) (Sakai et al., 1999) or bile acid-sensitive ion channel (BASIC) previously (Wiemuth et al., 2010), is restrictively expressed in the cerebellum and bile duct in the liver (Sakai et al., 1999). ASIC5 can be activated by bile acid in the bile duct, but the functional role of ASIC5 in the cerebellum is unclear (Boiko et al., 2014).

1d. Distribution of ASICs in the brain

In the brain, ASICs consist of homotrimeric ASIC1a and heterotrimeric ASIC1a/2a and ASIC1a/2b channels (Weng et al., 2010; Price et al., 2014). Immunostaining and Western blotting results in the previous studies indicate that ASIC1a, which is the principal subunit in a functional ASIC, is intense in olfactory bulb, cerebellar cortex, whisker barrel cortex, cingulate cortex, striatum, nucleus accumbens, hippocampus and amygdala. ASIC1a has the highest expression level in the amygdala (Wemmie et al., 2002; Wemmie et al., 2003; Price et al., 2014). In the hippocampus, multiple evidences suggest that ASIC current density is higher in GABAergic interneurons than that in glutamatergic pyramidal neurons (Bolshakov et al., 2002; Cho and Askwith, 2008; Ziemann et al., 2008). Moreover, the ASIC expression among hippocampal GABAergic inhibitory interneurons is cell type-specific, ASIC current

density of dendrite-targeting interneuron is six times greater than soma-targeting interneuron. And the subunit composition of ASICs in various classes of neurons is diverse (Weng et al., 2010). However, the cellular expression of ASICs in other brain regions is poorly understood.

In the subcellular level, ASICs might be located in the presynapse to modulate presynaptic release probability, which is increased in the hippocampus of ASIC1a knockout mice (Cho and Askwith, 2008). The other studies indicate that ASIC1a are located in somata and dendrites of pyramidal neurons of cortical and hippocampal cultures (Alvarez de la Rosa et al., 2003; Wemmie et al., 2003; Wemmie et al., 2006). Furthermore, a report indicates that the direct association between ASIC2a and postsynaptic density protein 95 (PSD-95) can interact with ASIC1a at dendritic spines, and these interaction influence postsynaptic spine number and sensitivity of acid (Zha et al., 2009). However, another immunohistochemical study suggested that ASIC1a might be present in membranes throughout neurons, including axons, with no preferential distribution to synapses (Alvarez de la Rosa et al., 2003). Even though the expression level of ASICs in the amygdala is the higher than other brain regions and many evidences show that ASICs are critical for fear learning and memory (Wemmie et al., 2002; Wemmie et al., 2003; Wemmie et al., 2006; Coryell et al., 2008; Coryell et

al., 2009; Ziemann et al., 2009), the distribution of ASIC subunits in the amygdala is still unclear.

1e. Gating properties of ASICs in the brain

In the brain, ASIC1a is the obligatory subunit (Wemmie et al., 2002; Wemmie et al., 2003). ASIC currents cannot be induced in the ASIC1a knockout mice (Wemmie et al., 2002; Askwith et al., 2004; Ziemann et al., 2008). ASIC2 plays modulatory role in a functional ASIC (Askwith et al., 2004; Sherwood et al., 2011). Homotrimeric ASIC2a can only be activated in vary acidic extracellular solution (pH 4.0) (Askwith et al., 2004). The different composition of ASICs have different gating properties. For instance, desensitization and recovery from desensitization are faster in ASIC1a/2a heterotrimers; Steady-state desensitization is larger in ASIC1a/2b heterotrimers (Askwith et al., 2004; Sherwood et al., 2011). Acid cannot induce a detectable ASIC current in the ASIC1a knockout mice (Wemmie et al., 2002; Askwith et al., 2004). The Phe-Met-Arg-Phe amide (FMRFamide) and related neuropeptides can enhance the sustained current of the ASIC1a-containing homo- and heterotrimers. The prolongation is extended in the ASIC1a/2a heterotrimer (Askwith et al., 2004). Some extracellular cations also influence the gating of ASICs. Zn^{2+} potentiates ASIC1a/2a, but inhibits

ASIC1a and ASIC1a/2b (Sherwood et al., 2011). High concentration of extracellular Ca^{2+} competes with H^+ for the binding site to attenuate the amplitudes of ASICs (Immke and McCleskey, 2003). Collectively, functional ASICs in brains, which are composed of ASIC1a homotrimer or ASIC1a/2 heterotrimer, can probably provide high pH-sensing diversity in various neural cells.

If. Physiological function of ASICs in the brain

In the physiological condition, the extracellular pH in the brain is tightly controlled by homeostatic mechanisms (Chesler and Kaila, 1992), but pH fluctuation in specific micro-domains is significant, such as synaptic cleft. Synaptic vesicle is acidified during packaging of neurotransmitter. The pH value of synaptic vesicle released during synaptic transmission is about 5.5, so the pH value can significantly drop in the synaptic cleft during neurotransmission and activate ASICs, which might present in the presynapses or postsynapses (Wemmie et al., 2002; Cho and Askwith, 2008; Du et al., 2014). A recent study shows that ASIC-dependent responses can be evoked by extracellular stimulation in the cortico-amygdala synapses with bath-application of synaptic blocker, CNQX and D-APV, which suggests that proton can act as neurotransmitter by activating the ASICs in the postsynapse (Du et al., 2014).

Increasing Ca^{2+} concentration by opening of Ca^{2+} permeable ASICs, including ASIC1a and ASIC1a/2b, activates Ca^{2+} /calmodulin-dependent protein kinases II (CaMKII) (Gao et al., 2005), and further facilitate long-term potentiation (LTP) through phosphorylation of NMDA receptor subtype 2B (NR2B)-containing NMDA receptors. In the hippocampus, the functional role of ASICs is controversial. A study revealed that NMDA-dependent LTP at CA3-CA1 synapses is impaired in the cultured hippocampal slice of ASIC1a knockout mice. They proposed that ASICs unblock Mg^{2+} on NMDA receptors at postsynapses to facilitate LTP (Wemmie et al., 2002). Results of Morris water maze suggest that ASIC1a null mice exhibit mild and reversible defects in spatial learning and memory. It might be because the impairment of LTP in the hippocampus of ASIC1a-null mice (Wemmie et al., 2003). However, the most recent studies show that LTP at CA3-CA1 synapse is not impaired in acute hippocampal slice of ASIC1a-null mice (Wu et al., 2013). Results of Morris water maze and Barnes maze also indicate that spatial learning is intact in the ASIC1a-null mice (Wu et al., 2013; Price et al., 2014). Consistent with this, CA1 pyramidal cells are expressing low level of ASICs (Weng et al., 2010).

Unlike hippocampus, amygdala is one of the brain regions that expressing high level of ASIC (Wemmie et al., 2003; Price et al., 2014). Multiple lines of evidence

indicates that ASICs can modulate the synaptic plasticity in the cortex → BLA synapses and promote the fear learning and memory. First, recent studies indicate that postsynaptic ASICs can be activated by presynaptic stimulation, especially with strong stimulation, like high-frequency stimulation (HFS) (Du et al., 2014; Kreple et al., 2014). Second, increasing the pH buffer capacity by HCO_3^- decreases the postsynaptic ASIC responses *ex vivo* (Du et al., 2014; Kreple et al., 2014), reduces the ASIC-dependent LTP at cortex → BLA synapses *ex vivo*, and impairs the fear-related behavior *in vivo* (Ziemann et al., 2009). Finally, disrupting ASIC1a in mice can reduce LTP of cortex → BLA synapses and conditioned fear (Wemmie et al., 2003; Du et al., 2014).

1g. ASICs in fear-related behaviors

Accumulating studies indicate that ASIC plays a critical role in the fear-related behaviors (Wemmie et al., 2003; Coryell et al., 2007; Du et al., 2014). Previous studies show that cued fear conditioning and contextual fear conditioning are impaired in ASIC1a null mice (Wemmie et al., 2003; Coryell et al., 2007). On the other hand, overexpression of ASIC1a increase acquired fear-related behavior (Wemmie et al., 2004). Furthermore, CO_2 inhalation can reduce the pH value in the amygdala and cause fear and anxiety (Ziemann et al., 2009). Loss or inhibition of ASIC1a impairs CO_2 -

induced fear behavior (Ziemann et al., 2009). Taken together, ASIC1a is important for fear learning and memory. Although ASIC1a protein is wide spread in many brain regions, in the previous immunohistochemistry study shows that amygdala has the most intense expression of ASIC1a (Wemmie et al., 2003). Moreover, restoring ASIC1a in the basolateral amygdala of ASIC1a knockout mice can rescue the contextual fear responses (Coryell et al., 2008). In contrast, ASIC1a in the amygdala did not contribute to unconditioned fear responses. Unconditioned fear responses are not impaired in ASIC1a knockout mice (Wemmie et al., 2003) or rescued by restoring ASIC1a in the basolateral amygdala (Coryell et al., 2008). Directly reducing pH to 6.8 in the amygdala by microinjection elicits fear behavior in mice (Ziemann et al., 2009). A recent report suggests that ASIC1a in the amygdala could be a therapeutic target in depression-related behavior (Coryell et al., 2009). However, how exactly ASIC1a within the intricate amygdala circuitry contributes to conditioned fear responses remains unknown.

1h. ASIC and diseases

ASICs involve in some neurological diseases, including ischemic stroke, epileptic seizure, and panic disorders (Wemmie et al., 2013). In several pathological conditions, like stroke, seizure, traumatic injury, and inflammation, brain cannot maintain the

extracellular pH value and cause acidosis (Wemmie et al., 2013). Prolonged and severe acidosis in the brain can result in acidosis-induced toxicity and neuronal death (Yermolaieva et al., 2004; Gao et al., 2005). Previous reports indicate that acidotoxicity in the brain is mediated by ASICs (Yermolaieva et al., 2004; Gao et al., 2005). Moreover, coupling between ASICs and NMDA receptors aggravate the ASIC-mediated acidotoxicity (Gao et al., 2005). The acid-induced cell death can be reduced by deleting ASIC1a or inhibiting ASICs by amiloride or PcTX1 (Gao et al., 2005).

However, a study shows that ASICs also have neuroprotection effect during early stage of seizure in the hippocampus (Ziemann et al., 2008). Deleting ASIC1a in mice increases the severity of seizure, whereas overexpressing ASIC1a in mice can shorten the duration of seizure (Ziemann et al., 2008). In the hippocampus, ASICs are largely expressed in the dendrite-targeting inhibitory interneurons but modestly expressed in the glutamatergic pyramidal cells (Bolshakov et al., 2002; Cho and Askwith, 2008; Ziemann et al., 2008; Weng et al., 2010). The activation of ASICs by acidosis increases the activity of inhibitory interneurons and reduces excitability of principal cells and seizures (Ziemann et al., 2008). But the cellular expression pattern of ASICs in other brain regions, such as amygdala, is unknown, whether ASICs have the same neuroprotection effect in other brain areas remains unclear.

ASIC1a is related to a very common psychiatric disorder, panic disorder (Smoller et al., 2014). The human ortholog of ASIC1a gene is associated with panic disorder and amygdala structure (Smoller et al., 2014). Repeating Panic attacks, which has shortness of breath and feeling of suffocation, is the symptom of panic disorder. Inhalation of 35% CO₂ (with 65% O₂) can trigger panic attacks in most patients with panic disorders (Battaglia and Perna, 1995; Battaglia et al., 2005). In keeping with this, inhalation of 20% CO₂ (With 21% O₂, balanced with N₂) significantly reduces amygdala pH to 6.7 and induces fear responses in mice (Ziemann et al., 2009). Moreover, the CO₂-induced fear responses can be reduced by disrupting ASIC1a in mice and be rescued by restoring ASIC1a in ASIC1a-null mice (Ziemann et al., 2009). Collectively, ASICs involve in panic disorder and amygdala dysfunction, but the underlying mechanism remains to be answered.

2. Amygdala Network

2a. Center of fear learning and memory

Fear and anxiety are very common emotion in human and all mammals, and appear to be a kind of survival strategy by initiating avoidance or escape from predators and harmful situation. Abnormal fear and anxiety can cause many psychiatric diseases, such

as generalized anxiety disorder, phobic disorder and panic disorder. Despite the high prevalence of fear and anxiety disorders, the molecular/cellular mechanisms and the underlying fear circuitry are poorly understood. Pavlovian fear conditioning is an important animal model, and has become a standard task for investigate the acquired fear. In Pavlovian fear conditioning, conditional stimulations (CSs) such as auditory tones, lights, or places are arranged to predict the following aversive unconditional stimulation (US), such as foot shock. After fear conditioning, CSs can evoke learned fear responses, like freezing (Maren, 2008). Moreover, Pavlovian conditioned fear response can also be reduced by fear extinction. Extinction occurs when the relation between CSs and learned fear response is broken by exposures to the CSs in absence of US. Studying the mechanism of fear conditioning and fear extinction can help us to understand the role of fear circuitry, and may benefit the development of drugs used to treat anxiety and fear disorders.

Amygdala, an almond-shape structure located in the medial temporal lobe, has been shown to be the central of acquisition, storage, and expression of fear-related behaviors (LeDoux, 2000; Ehrlich et al., 2009; Paré and Duvarci, 2012; Duvarci and Paré, 2014). Amygdala is a complex structure which can be separated into several nuclei, basolateral amygdala (BLA), central amygdala (CeA), intercalated cell masses

(ICMs). The CeA can be further divided into lateral part (CeL) and medial part (CeM) (Figure 1; LeDoux, 2000; Ehrlich et al., 2009). Among them, BLA is cortex-like nuclei which contains primarily glutamatergic principal neurons, others are striatum-like structure which consist of a majority of GABAergic neurons. All nuclei form a complex microcircuitry to processing the fear learning and memory.

2b. Basolateral amygdala (BLA)

BLA, which is the combination of lateral amygdala (LA) and basal amygdala (BA), is the first input station of fear learning circuitry (Figure 1a; LeDoux et al., 2000; Ehrlich et al., 2009). Many evidences indicate that BLA is critical for acquisition, storage and expression of fear memory (LeDoux, 2000; Goosens and Maren, 2001; Duvarci and Paré, 2014). Lesion of BLA can cause the impairment of fear conditioning (LeDoux, 2000; Goosens and Maren, 2001). As a cortex-like structure, BLA consists majority of glutamatergic principal neurons (PNs) (approximately 80%) and minority of GABAergic interneurons (INs) (approximately 20%) (Ehrlich et al., 2009; Duvarci et al., 2011). BLA-PN receives and integrates the CS and US information from cortex and thalamus input and outputs to the downstream brain regions (Ehrlich et al., 2009; Paré and Duvarci, 2012). Previous reports show that fear conditioning can enhance

synaptic plasticity in the BLA (Rogan et al., 1997; McKernan and Shinnick-Gallagher, 1997). LTP is considered as the underlining mechanism of learning and memory (Shin et al., 2006).

The minority neuron population, GABAergic INs, has greater diversity than PNs in the BLA. Various GABAergic INs in the BLA are also involved in the fear learning and memory by manipulating the excitability of PNs (Figure 1a and 1b; Ehrlich et al., 2009; Wolff et al., 2014). Similar to cortex or hippocampus, different groups of GABAergic INs expressing specific Ca^{2+} binding protein or neuropeptides (Spampanato et al., 2011). There are two major classes of INs in the BLA, parvalbumin-expressing IN (PVIN), a classical type of soma-targeting IN, and somatostatin-expressing IN (SOMIN), a major type of dendrite-targeting INs (Wolff et al., 2014). A recent study indicates that PVINs are activated during auditory fear conditioning and indirectly disinhibit the PNs via SOMINs, thereby enhancing auditory responses and promoting cue–shock associations (Wolff et al., 2014). During an aversive footshock, however, both PVINs and SOMINs are inhibited, which boosts postsynaptic footshock responses and gates learning (Wolff et al., 2014). Thus, PVINs and SOMINs are playing different role in the fear conditioning. Moreover, PVINs also play a role in the extinction of fear memory. During fear extinction, the silencing of BLA-PNs is cause

by the increasing of the perisomatic inhibitory synapses projected from PVINs to PNs (Trouche et al., 2013). The GABAergic INs in the BLA can also be classified by expression of other Ca^{2+} binding protein or neuropeptides, including calbindin, calretinin, cholecystokin, and vasoactive intestinal peptide-expressing. However, the activity and contribution of these GABAergic INs in the fear learning and memory is poorly understood.

2c. Central amygdala (CeA)

In contrast to BLA, CeA is a striatum like structure which composes majority of GABAergic neurons (Ehrlich et al., 2009). CeA can be divided into two subdivision, lateral part (CeL) and medial part (CeM) (Figure 1b). CeL accept excitatory input from BLA and lateral parabrachial nucleus (lPB) and inhibitory projection from medial-dorsal ICM (ICM_{MD}) (Ehrlich et al., 2009; López de Armentia and Sah, 2007). The activation of CeL neurons modulate the CeM output neurons, the principal output station of fear learning circuitry. There are two groups of GABAergic neurons in the CeL, CeL_{off} and CeL_{on} neurons, which have different neuronal activity during fear response and have distinct cell marker, protein kinase C- δ (PKC- δ), and SOM (Haubensak et al., 2010; Cioocchi et al., 2010; Duvarci et al., 2011; Li et al., 2013).

CeL_{off} neurons, which are expressing PKC- δ but not SOM, project an inhibitory synapse onto CeM output neurons and reduce fear response by silencing of CeM output neurons (Haubensak et al., 2010; Ciochi et al., 2010) (Figure 1b). In contrast, CeL_{on} neurons, which are expressing SOM but not PKC- δ , can inhibit CeL_{off} neurons and cause disinhibition in the CeM output neurons (Li et al., 2013) (Figure 1c). The activation of CeL_{on} neuron cause freezing responses (Li et al., 2013).

The primary output neurons of fear learning circuitry are mainly in the CeM (Figure 1b; Ehrlich et al., 2009; Viviani et al., 2011; Duvarci and Paré, 2014), which project to the hypothalamus and brain stem that implicate in autonomic and motor-related responses of fear behaviors (Viviani et al., 2011). CeM accept excitatory input from BLA and inhibitory input from CeL and medial-ventral ICM (ICM_{MV}) (Ehrlich et al., 2009). Lesion of CeM or reduce the activity of CeM neurons by pharmacological approach leads to impairment of fear learning and memory (Goosens and Maren, 2001; Ciochi et al., 2010).

2d. Intercalated cell masses (ICMs)

ICMs is clusters of small GABAergic neurons surrounding the BLA (Figure 1b). ICMs play a modulatory role in the fear circuitry, which are critical in the fear extinction.

Both ICM_{MV} and ICM_{MD} are clusters of GABAergic neurons between the BLA and CeA, receiving input from the BLA and sending feedforward inhibitions to the CeA. But ICM_{MV} and ICM_{MD} play distinct role in the fear circuitry. ICM_{MV} neurons directly inhibit the CeM output neurons (Figure 1b). In contrast, the ICM_{MD} neurons plays a similar disinhibition role like CeL_{on} neurons, which can increase the activity of CeM neurons by projecting inhibitory synapses onto CeL_{on} neurons and ICM_{MV} (Duvarci et al., 2014). On the other hand, the lateral ICM (ICM_L) is located on the dorsal–lateral side of the BLA, projecting inhibitory outputs to the BLA (Figure 1b).

2e. Fear learning circuitry

In the fear conditioning, after BLA-PNs receive input from cortex or thalamus, there are several downstream pathway in the amygdala network are involved in the fear conditioning (Figure 1b). First, BLA-PNs can directly activate CeM output neurons by sending glutamatergic projection to CeM output neurons. Second, BLA-PNs can indirectly increase the activity of CeM neurons by disinhibition. The glutamatergic projection from BLA to CeL_{on} neurons and ICM_{MD} inhibit the CeL_{off} neurons and ICM_{MV} and disinhibit CeM output neurons. Finally, the CeM neurons send output to

the hypothalamus and brain stem which are correlated to fear behaviors (Figure 1b; Ehrlich et al., 2009; Viviani et al., 2011; Duvarci et al., 2014).

There are strong evidences indicate that fear extinction does not reverse or erase the memory of learned fear but form a new memory that inhibit the original fear memory (Myers and Davis, 2007). There are several types of neurons are participate in the fear extinction pathway which can inhibit the fear conditioning pathway. First, BLA-PNs, which are activated during fear conditioning, are silenced by GABAergic INs and ICM_L (Figure 1c; Likhtik et al., 2008; Amano et al., 2011). Second, CeL_{off} neurons form an inhibitory synapse to CeM output neurons (Figure 1c; Haubensak et al., 2010; Cioocchi et al., 2010). Finally, two reports show that there are 15% of PNs in the BLA are related to fear extinction, which are named as “extinction cells” (Figure 1c; Herry et al., 2008; Popescu and Paré, 2011). The activation of extinction cells in the BLA can activate the ICM_{MV} and send a feedforward inhibition to CeM output neurons (Figure 1c; Herry et al., 2008; Popescu and Paré, 2011; Duvarci and Paré, 2014).

Overall, fear behavior is caused by a very complex networks in the amygdala. The behavior observed in fear conditioning and extinction is dependent on the manipulation of CeM, the final output station of fear circuitry which can directly govern the fear

responses output neurons, by multiple pathway in the fear circuitry (Figure 1b and 1c; Ehrlich et al., 2009; Duvarci and Paré, 2014).

3. *Specific aims*

ASIC has been proposed to be the therapeutic target of panic disorder. Despite the importance of ASIC in the fear learning and memory and high expression level of ASIC in the amygdala. The functional expression and role of ASIC in each types of amygdala neurons are poorly understand. Here, we are going to exam the expression and functional role of ASIC in the amygdala network from cellular level, synaptic level to behavioral level.

3a. Aim 1: Functional expression and properties of ASICs in amygdala neurons.

The amygdala is composed of several subnuclei that can be classified into two groups, cortex- and striatum-like structures. Each subnucleus comprises heterogeneous populations of neurons. Despite the importance of ASIC in amygdala circuitry, the expression pattern and properties of ASIC in distinct types of amygdala neurons remain largely unknown. Using whole-cell recording and glutamic acid decarboxylase 67-green fluorescent protein (GAD67-GFP) knock-in (KI) mice, we will classify

electrophysiological properties of different cell types in various nuclei of amygdala network. To measure the expression and properties of ASIC in the amygdala network, we will first exam pH dependency and Na⁺ permeability of ASIC in the BLA-PNs. Second, the composition of ASICs will be tested by genetic deleting of ASIC1a or ASIC2 and pharmacologic approach. Finally, the functional expression and properties of ASIC in most cell types in various nuclei of the amygdala network will be measured by nucleated patch recording and fast-application system.

3b. Aim 2: Functional role of ASICs in multiple glutamatergic synapses.

Activity-induced LTP of cortico-BLA synapses is impaired in ASIC1a-null mice, suggesting a critical role of ASICs in synaptic plasticity. However, whether ASIC is required for synaptic plasticity in different glutamatergic synapses in the amygdala circuitry remains unclear. Using ASIC1a conditional knockout mice with Cre/loxP system, the contribution of ASIC in LTP of multiple glutamatergic synapses will be determined by whole-cell recording and extracellular stimulation.

3c. Aim 3: The contribution of ASICs in different cell types to fear behavior.

Although multiple evidence indicate that ASIC in the amygdala is critical for learned fear, whether the expression of ASIC in different cell types are required for fear learning and memory is not clear. Here, we will selectively delete ASIC1a in different cell types by Cre/loxP system to examine the contribution of ASICs in conditioned fear.



Chapter 2

Functional Expression and Roles of ASICs in Amygdala Network

Introduction

The amygdala is a complex structure in the mid-temporal lobe that plays a key role in fear learning and emotional processing (LeDoux, 2000; Ehrlich et al., 2009; Duvarci and Paré, 2014). Gene variations in *ACCN2*, the human ortholog of *ASIC1a* gene, are associated with both panic disorder and alterations in human amygdala structure and function (Smoller et al., 2014). Several lines of evidence implicates that ASICs in the rodent amygdala contribute to fear-like behavior. First, deletion of *ASIC1a*, the principal subunit of functional ASIC in the brain, in mice impaired conditioned fear behavior and innate fear (Wemmie et al., 2003). Second, restoring *ASIC1a* in the basolateral complex of amygdala (BLA) of *ASIC1a*-null mice rescues the fear memory (Coryell et al., 2008). Third, overexpression of *ASIC1a* increases acquired fear-related behavior (Wemmie et al., 2004). Finally, ASICs contribute to LTP at cortico-BLA

synapses, and this synaptic plasticity was shown to be critical for associative fear learning and memory (Du et al., 2014).

Although ASICs are expressed widely in the brain, ASIC1a and ASIC2 are particularly enriched in the amygdala (Wemmie et al., 2003; Price et al., 2014). The amygdala comprises a heterogeneous collection of nuclei, including the BLA, CeA, and ICMs (LeDoux, 2000; Duvarci et al., 2014; Sah et al., 2003). Fear conditioning is known to cause widespread synaptic plasticity in the amygdala circuitry (Shin et al., 2006; Sah et al., 2008; Fourcaudot et al., 2009). Despite the importance of ASICs in the cortico-BLA for fear learning, it is not clear whether the distribution of ASICs varies among different cell types within amygdala circuits, or whether synaptic plasticity in other cell types depends on ASICs and such plasticity also plays a role in fear learning.

To address these questions, we initiated by measuring ASIC currents in different types of amygdala neurons. We used *GAD67-GFP* KI mice (Tamamaki et al., 2003) to differentiate glutamatergic principal neurons (PNs) and GABAergic neurons. ASIC current densities and their gating properties were measured by the nucleated patch recording and fast application technique (Lien et al., 2002; Weng et al., 2010). Using these approaches, we found that ASIC expression was highly cell type- and region-specific, whereas ASIC gating kinetics and subunit composition were similar. Notably,

ASICs were highly expressed in glutamatergic PNs of the BLA, which is receiving cortical and thalamic inputs, and low-threshold bursting (LTB) GABAergic neurons in the CeM, which is the output station of the amygdala circuitry. This result suggests that the contribution of ASIC in the fear-related behavior might in the input and output station of amygdala network. Analysis of synaptic plasticity revealed that the abundance of ASICs in postsynaptic neurons correlated with, and contributed to, LTP of glutamatergic synapses. Importantly, although LTP at cortico-BLA synapse are remained when ASIC1a is selectively deleted in the GABAergic neurons by Cre/loxP recombinant system, LTP at intra-amygdala synapses onto output neurons is significantly reduced in mice with selective deletion of ASIC1a in GABAergic neurons.

The LTP is considered to be the underlying mechanism of learning and memory. We further investigate whether the high expression level of ASICs in these cell types is required for fear conditioning. By selectively deleting ASIC1a in the BLA-PNs or GABAergic neurons with Cre/loxP system, we found that conditioned fear is impaired in both ASIC1a deletion in BLA-PNs and GABAergic neurons. Collectively, ASIC-dependent LTP at both cortico-BLA input synapses and intra-amygdala synapses on output neurons are critical for fear learning and memory.

Materials and Methods

Brain slice preparation

Coronal brain slices (300 μm thick) were prepared from mice (9–75 days old for AISC characterization; 1–4 months old for LTP experiments and 3–5 months old for behavioral tests) of either sex on C57BL/6 genetic background, including wild-type (WT), *GAD67-GFP* KI, *ASIC1a*^{-/-}, and *ASIC2*^{-/-} mice, using a vibratome (DTK-1000, Dosaka, Kyoto, Japan), as described previously (Lien et al., 2002). Animals were killed by decapitation, in accordance with national and institutional guidelines, and all procedures were approved by the Animal Care and Use Committee of National Yang-Ming University. Floxed *ASIC1a* (*ASIC1a*^{fl/fl}) mice were crossed with *Nestin-Cre* and *GAD65-Cre* transgenic mice to generate *ASIC1a* gene deletion in their offspring (Wu et al., 2013). *ASIC2*^{-/-} mice (Price et al., 2000) were obtained from Jackson Laboratory (Bar Harbor, ME, USA). To facilitate cell type identification, we used *GAD67-GFP* KI mice, in which GFP expression was driven by the *GAD67* promoter (Tamamaki et al., 2003). Slices were sectioned in ice-cold cutting solution containing (in mM): 87 NaCl, 25 NaHCO₃, 1.25 NaH₂PO₄, 2.5 KCl, 10 glucose, 75 sucrose, 0.5 CaCl₂ and 7 MgCl₂. Following sectioning, slices were incubated in the cutting solution (oxygenated with

95% O₂/5% CO₂) in a holding chamber at 34°C for 30 min, and then at room temperature until used. During experiments, individual slices were transferred to a submersion recording chamber and were continuously superfused with oxygenated artificial cerebrospinal fluid (CSF) containing (in mM): 125 NaCl, 25 NaHCO₃, 1.25 NaH₂PO₄, 2.5 KCl, 25 glucose, 2 CaCl₂ and 1 MgCl₂. The recording temperature was 25 ± 3°C. Neurons were visualized under the guidance of infrared differential interference contrast (DIC) optics and by their green fluorescence with epifluorescence illumination.

Nucleated patch recordings

Nucleated patch recordings were made, as described previously (Lien et al., 2002; Lien and Jonas, 2003), using an Axopatch 200B amplifier (Molecular Devices, Sunnyvale, CA, USA). Pipette capacitance was compensated. Signals were low-pass filtered at 5 kHz (four-pole Bessel) and sampled at 10 kHz using a digitizer (Digidata 1440A; Molecular Devices). Pulse sequences were generated by a Digidata 1440A via pClamp 10.2 (Molecular Devices). Minor and major axes of nucleated patches were measured. It was assumed that nucleated patches were approximately ellipsoid (Gentet et al., 2000), and the membrane surface area was calculated using the following formula:

$$\text{Surface area} = \frac{(\text{major axis} + \text{minor axis})^2 \pi}{4} \quad (1)$$

The total membrane capacitance was determined from the surface area, using the value ($1 \mu\text{F}/\text{cm}^2$) of specific membrane capacitance (Gentet et al., 2000; Chan et al., 2013). Fast application of H^+ on nucleated patches, isolated from identified neurons, was performed, as described previously (Weng et al., 2010). Fast application experiments were started 1–2 min after the patches were excised. Double-barreled application pipettes were fabricated from theta glass capillaries (2 mm outer diameter, 0.3 mm wall thickness, 0.12 mm septum, Hilgenberg GmbH, Malsfeld, Germany) and mounted on a piezoelectric-based solution switching system (MXPZT-300, Siskiyou, OR, USA). The time necessary for the complete exchange of solutions was determined using an open patch pipette by switching between Na^+ -rich and 10% Na^+ -rich solutions, which was $186 \pm 14 \mu\text{s}$ ($n = 3$) by measuring 20–80% rise time of the junction potential change. ASIC currents evoked by 1 s pulses of H^+ were applied every 20 s, except for some pharmacological experiments where short pulses (50 ms) were used.

To evoke ASIC currents with various pH values, 2-(*N*-morpholino)ethanesulfonic acid (MES)-buffered Na^+ -rich external solution in the test barrel was used, containing (in mM): 135 NaCl, 5.4 KCl, 1.8 CaCl_2 , 1 MgCl_2 , 10 MES, adjusted to the desired

values with *N*-methyl-D-glucamine. The intracellular solution contained (in mM): 142 K-gluconate, 2 KCl, 0.2 EGTA, 4 MgATP, 10 HEPES, 7 Na₂-phosphocreatine; pH adjusted to 7.3 with KOH. Bovine serum albumin (0.1%) was added to external solutions containing the spider toxin PcTX1 (Peptides International, Louisville, KY, USA) to prevent its absorption into tubing and containers. For PcTX1 application, both pH 7.4 and 5 external solutions contained 30 nM PcTX1. The nucleated patches were placed in the pH 7.4 solution at least 1 min before the fast-application experiment. All other chemicals were from Sigma (St. Louis, MO, USA), unless specified otherwise.

Immunohistochemistry

For immunofluorescent labeling, brains were removed from *GAD67-GFP* KI mice which were transcardially perfused with 4% paraformaldehyde in 0.1 M phosphate buffered saline (PBS). Brains were further dehydrated in 15% sucrose for 24 h, and 30% sucrose for 24 h. Cryostat sections (20 μm thick) were rehydrated with PBS. Following a PBS wash, sections were permeabilized with 0.3% PBST (0.3 % triton-X-100 in PBS) for 30 min and incubated in 10% normal goat serum (NGS) for 2 h to block non-specific binding. To stain NeuN, which is a neuron-specific protein, sections were incubated in primary mouse anti-NeuN antibody (1:400; MAB377; Merck Millipore,

Billerica, MA, USA) with 5% NGS in 0.3% PBST for 24 h at 4°C. Following a PBS wash, sections were incubated in secondary antibody (goat anti-mouse Alexa Fluor 594; Life Technologies, Grand Island, NY, USA) with 2% NGS in 0.3% PBST for 2 h at 4°C. Following a PBS wash, sections were mounted in VECTASHIELD HardSet Mounting Medium (Vector Laboratories, Burlingame, CA, USA) and viewed under a Zeiss Microscope Axio Observer A1 (Zeiss, Oberkochen, Germany).

Hierarchical clustering analysis

For cell classification, unsupervised clustering (Cauli et al., 2000; Jasnow et al., 2009; Sosulina et al., 2010) was performed, using squared Euclidean distances and Ward's method (Ward, 1963). Electrophysiological properties of BLA INs and CeL neurons were tested for uniformity in their distributions. Variables with a nonuniform distribution were used for subsequent unsupervised clustering. Hierarchical clustering was operated, as follows. First, each neuron was transformed into a four-dimensional data point with variables. Before clustering, variables were first normalized into the range (0, 1) by performing Min-max normalization. The distance between data points represented the dissimilarity between them; closer data points have higher similarity. Next, all the data points were clustered by the following iterative procedure. First, each

data point was assigned to a cluster; every cluster therefore contained only one data point. Second, the two closest clusters were merged into one cluster, such that there would be one fewer cluster. Third, the distance between the new cluster and each of the old clusters was determined. Fourth, steps two and three were repeated, until there was only one cluster left. Ward's method linkage rules (Ward, 1963) minimize the error sum of squares of any pair of cluster in step three. The pair of clusters with a minimum between-cluster distance was merged. The hierarchical clustering analysis was carried out using Free Statistics Software v.1.1.23-r7 (Wessa, 2014).

Measurement of synaptic responses and LTP induction

Excitatory postsynaptic potentials (EPSPs) or currents (EPSCs), in the presence of GABA receptor type A (GABA_AR) antagonist gabazine (1 μ M), were recorded from identified neurons in current or voltage clamp. Basal synaptic responses were evoked by a brief pulse (0.1–0.5 ms) of either constant voltage or current delivered by a stimulus isolation unit (Isoflex, A.M.P.I., Jerusalem, Israel) every 20 s with tungsten bipolar electrodes. Stimulation electrodes were positioned at axonal bundles of inputs of interest. Synaptic strength was quantified as the peak amplitude of EPSP or EPSC. Baseline responses were collected with a stimulation intensity that yielded 10–30% of

the maximal response. Slices displaying unstable baseline recording or series resistance change of $> 20\%$ were discarded. For the cortex \rightarrow BLA-PN synapse, LTP was induced by pairing four trains of HFS (HFS \times 4, 100 Hz for 1 s per train; 10 s intervals) with brief supra-threshold current step injections (approximately 2 nA; 1 ms) into the postsynaptic cell (with a 5 ms delay) in a current clamp (Shin et al., 2006). For the BLA \rightarrow CeM neuron synapse, LTP was induced by HFS \times 4 (10 s intervals), with postsynaptic cells held at -70 mV in a current clamp (Fu et al., 2007). Similarly, HFS \times 4 (20 s intervals), with postsynaptic cells held at -50 mV, was used to induce LTP at the IPB \rightarrow CeL neuron synapse (López de Armentia and Sah, 2007).

Fear conditioning

Fear conditioning was performed in two different contexts. On day 1, mice were placed into the conditioning box (context A) for 2 min habituation and then received five trials of tone (80 dB, 20 s)-foot shock (0.6 mA, 2 s) pairings. A foot shock was given 2 s before the end of a tone. There was 1 min observation time between each pairing. To evaluate fear learning, we recorded the freezing time during habituation and between each trial. The context-dependent fear memory test was performed 24 h later by re-exposing the mice for 5 min to context A. One hour later, mice were placed into

context B for 2 min, which was followed by three trials of 20 s tone plus 1 min observation time to evaluate the tone-dependent fear memory. We recorded the freezing time to context or tone during the total observation time. Freezing is defined as a lack of movement (> 2 s) associated with a crouching posture, except for heartbeat and respiration. The freezing time is expressed as a percentage of the total observation time.

Virus injections

Mice (2–4 months old) were anaesthetized with isoflurane and placed into a stereotaxic frame (Stoelting, Wood Dale, IL, USA), with the mouths and noses covered by the anaesthetizing mask with constant air flow containing 1.5% isoflurane (air flow rate: 4 mL/min). The mice were placed over a homeothermic blanket (Panlab Harvard apparatus, Barcelona, Spain) to keep their body temperature constant (36°C), with their eyes protected by ophthalmic gel during securing. The skull was surgically exposed using scissors and drilled over the desired coordinates. AAV8-CMV-GFP was generated in the laboratory of our collaborator Dr. Min-Hong Tai (National Sun Yat-Sen University, Taiwan). The transgene (pAAV-CMV-GFP), packaging (pLT-RC08), and helper (pHGTI-aden01) constructs were gifts from Dr. Jeng-Shin Lee (Harvard Gene Therapy Initiative, Harvard Medical School, Boston, MA, USA). AAV2/8 was

serotyped with AAV8 capsid proteins. The AAV8-CaMKII α -GFP-Cre was purchased from University of North Carolina Vector Core (Chapel Hill, NC, USA). The virus was delivered through the craniotomy bilaterally using a 10 μ L NanoFil syringe (World Precision Instruments, Sarasota, FL, USA) and a 35-gauge beveled metal needle. The injection volume (0.5 μ L at each location) and flow rate (0.1 μ L/min) were controlled with a nanopump Controller (KD Scientific, Holliston, MA, USA). The needles were left in position for 10 min after injection. Injection coordinates, relative to Bregma, were: anterior–posterior, -2 mm; medial–lateral, ± 3.4 mm; dorsal–ventral, -5 mm and -5.1 mm. Mice were allowed to recover for 3 weeks, following injection.

Data analysis and statistics

Data were analyzed and fitted with Clampfit 10.0 (Molecular Devices) and Prism 5.01 (GraphPad, La Jolla, CA, USA). The accommodating ratio is the maximal ratio of the mean of the last five inter-spike intervals (ISIs) divided by the mean of the first five ISIs under minimal current step injection (< 400 pA) which could generate > 10 APs per second. The spike delay is the latency of the first AP upon 1 s near-threshold depolarizing (rheobase) current step injection. The ISI ratio is calculated as the latter ISI divided by the previous ISI. The maximal coefficient of variation (CV) of ISI ratios

was calculated from spike trains evoked by 1 s current step injection. The maximal mean firing rate is the maximal number of APs that could be generated by 1 s current step injection. Input resistance is defined by the ratio of steady-state voltage change/1 s hyperpolarizing current (−25 pA or −50 pA). For classification of BLA GFP-expressing cells, four features consisting of the accommodating ratio, maximal CV of ISI ratio, delay, and maximal mean firing rate were used to identify different cell types. The desensitization time constant of ASIC current was obtained by fitting currents with the function shown below:

$$I(t) = Ae^{-\frac{t}{\tau}} + C \quad (2)$$

A denotes the peak amplitude of current, τ represents the desensitization time constant, and C denotes the amplitude of steady-state current.

The pH-response curve was fitted with the function, as shown below:

$$f(c) = \frac{A}{\left[1 + \left(\frac{EC_{50}}{c}\right)^n\right]} \quad (3)$$

where A is the constant for the maximal effect, c denotes the concentration, EC_{50} represents the half-maximal effective concentration, and n denotes the Hill coefficient.

For reversal potential measurements, data points of I - V relations were fitted with second-order polynomials, from which the interpolated potentials were calculated. The theoretical reversal potential of sodium channels (E_{Na}) was calculated, according to the Nernst equation:

$$E_{Na} = \frac{RT}{F} \ln \frac{[Na^+]_o}{[Na^+]_i} \quad (4)$$

where $[Na^+]_o$, $[Na^+]_i$ are outer and inner Na^+ concentrations, and F , R , T have standard thermodynamic meanings (Hille, 2001).

Values indicate mean \pm s.e.m. (standard error of mean); error bars in Figures also represent s.e.m. Statistical significance among groups was tested using the nonparametric Kruskal-Wallis test. Where significant, pairwise comparisons, using the Wilcoxon rank-sum test, were carried out for each pair of groups. Statistical significance of linear regression was tested using the F-test. All tests were performed at the significance level (P) as indicated. The s.e.m. of reversal potentials were obtained by analyzing data of individual experiments separately.

Results

GABAergic neurons are identified by GAD67-GFP knock-in mice

The amygdala is composed of several synaptically interconnected nuclei (Ehrlich et al., 2009; Paré and Duvarci, 2012; Duvarci and Paré, 2014). As illustrated in Figure 2a1, the borders of individual nuclei in a coronal section of the mouse brain were outlined and neurons were identified with the neuronal marker NeuN. Like in most regions of mammalian brain, glutamatergic and GABAergic cells account for the majority of neurons in the amygdala. Here, we used the *GAD67-GFP* KI mouse to differentiate between GABAergic and non-GABAergic neurons (Figure 2a2, 2a3). Previous immunohistochemical studies in various brain regions have verified that GFP⁺ cells in this mouse are GABAergic (Tamamaki et al., 2003). As previously reported (McDonald, 1982; Sah et al., 2003; Ehrlich et al., 2009; Paré and Duvarci, 2012), the BLA consists of a majority (~80%) of glutamatergic PNs (Figure 2b) and a minority (~20%) of sparsely GABAergic INs (Figure 2b). In contrast with the above, the CeA, consisting of the CeL and CeM, is composed of mostly (~90%) GAD67-GFP labelled cells (Figure 2c and 2d). Likewise, the ICMs are made of densely packed GABAergic cell clusters (Figure 2a and 2e). The ICMs comprise of three clusters and are referred

to as the ICM_L, ICM_{MD}, and ICM_{MV}, respectively, according to their locations (Duvarci and Paré, 2014).

Cell type-specific expression of ASICs in the BLA

To investigate the functional expression of ASICs, we used fast application of proton (H⁺) to excised nucleated patches from recorded neurons (Figure 3a). As previously described (Lien et al., 2002; Lien and Jonas, 2003; Weng et al., 2010), nucleated patch recording provides three major advantages in this study. First, it allows rapid application of proton, suitable for studying rapidly desensitizing ASICs. Second, it provides an almost ideal space-clamp, allowing precise measurement of ASIC current kinetics. Third, it provides reliable measurement of current density, facilitating comparison among multiple neuronal subtypes. Solution exchange could be achieved in less than 200 μs (see Material and Methods) with our fast application system. We found that BLA-PNs generated regular and accommodating action potential (AP) trains, in response to depolarizing current pulses in the current clamp (Figure 3b, top). Nucleated patches from BLA-PNs exhibited ASIC-like, transient inward currents (Figure 3b, bottom), in response to a submillisecond switch of extracellular pH from

7.4 to 5. The peak amplitude of the current depended on the pH value of the applied solution (Figure 3c).

ASICs are non-voltage-gated Na⁺ channels, preferentially permeable to Na⁺ (Waldmann et al., 1997). We next determined the reversal potential of ASIC-like currents in BLA-PNs by measuring currents at different holding potentials (Figure 3d, top). The *I-V* relationship showed that ASIC-like currents reversed at 67.8 ± 5.2 mV ($n = 6$; Figure 3d), close to the Na⁺ equilibrium potential (61 mV) under the recording condition. The responses (to pH 5) measured at -65 mV were independent of animal ages (19 to 30 days, 152 ± 4.5 pA/pF, $n = 14$; 30 to 60 days; 139 ± 28 pA/pF, $n = 10$; 60 to 75 days, 131 ± 8 pA/pF, $n = 3$; $P = 0.50$, Kruskal–Wallis test) and thus were pooled together in this study. Using *ASIC1a*^{-/-} (*Nestin*^{Cre/+}; *ASIC1a*^{fl/fl}, Figure 4a) and *ASIC2*^{-/-} mice, we found that a pH fall from 7.4 to 5 induced large current in WT mice (178 ± 14 pA/pF, $n = 28$; Figure 4b) but did not activate detectable currents in *ASIC1a*^{-/-} mice (3.0 ± 0.6 pA/pF, $n = 5$; Figure 4b), while these currents were greatly reduced in *ASIC2*^{-/-} mice (*ASIC2*^{-/-}, 45.4 ± 4.5 pA/pF, $n = 6$; *** $P < 0.001$, Wilcoxon rank-sum test; Figure 4b). This results consistent with the obligatory role of the ASIC1a subunit for a functional ASIC (Askwith et al., 2004) and the auxiliary role of ASIC2 (Zha et al., 2009). Furthermore, we found that although the desensitization time constant (τ) was

unchanged (Figure 4c, bottom left), the current amplitude in *ASIC2*^{-/-} mice showed a significantly accelerated reduction during repeated stimulation (Figure 4c, top and bottom right). Finally, these currents were significantly reduced by PcTX1 (control, 357 ± 38 pA; PcTX1, 268 ± 34 pA, n = 11; ***P < 0.001, Wilcoxon signed-rank test; Figure 4d), a specific peptide blocker of ASIC1a homomeric, and ASIC1a/2b heteromeric, channels (Chen et al., 2005; Sherwood et al., 2011). Together, these results indicate that proton-activated currents in BLA-PNs were mediated by ASIC1a, ASIC2a, and ASIC2b subunits. Owing to the weak sensitivity to PcTX1, a large proportion of current was likely mediated by ASIC1a/2a heteromers.

GABAergic INs in the BLA display heterogeneous intrinsic excitability (Table 1; Sosulina et al., 2010; Song et al., 2013). To avoid arbitrary and subjective classification, we performed hierarchical cluster analysis (Ward, 1963) from randomly recorded GFP-expressing cells in the BLA of *GAD67-GFP* KI mice. Variables with nonuniform distribution (Figure 5a to 5d) were used for subsequent unsupervised clustering (Figure 5e). Four major IN subtypes were identified, including accommodating INs (AcINs), stuttering INs (StINs), delay-firing INs (DFINs), and fast-spiking INs (FSINs) (Figure 5; see Materials and Methods). Among these, AcINs exhibited an accommodating AP pattern (Figure 5f); StINs exhibited a characteristic pattern of multiple AP bursts

separated by variable quiescent periods (Figure 5g); DFINs exhibited a marked spike delay in response to near-threshold current pulse injection (Figure 5h); and FSINs showed characteristic brief APs with high firing rates and little accommodation (Figure 5i). Nucleated patch measurements from these cells showed that AcINs, StINs, and DFINs exhibited large ASIC currents (Figure 6a to 6c), similar to BLA-PNs, while FSINs showed very small ASIC currents (Figure 6d). Thus, ASIC expression in GABAergic INs in the BLA is cell type-specific (PN, 150 ± 13 pA/pF, $n = 30$; AcIN, 136 ± 32 pA/pF, $n = 9$; StIN, 131 ± 41 pA/pF, $n = 10$; DFIN, 114 ± 36 pA/pF, $n = 5$; FSIN, 8.9 ± 3.2 pA/pF, $n = 6$; Figure 6e).

Cell type- and subregion-specific ASIC expression in the CeA

The CeA, which contains CeL and CeM, receives excitatory inputs from the BLA and inhibitory projections from the ICM_{MD} and ICM_{MV} (Duvarci and Paré, 2014). Previous studies have identified two major types ('late-spiking' [LS] and 'early-spiking' [ES]; Figure 7a and 7b; Table 2) of GABAergic neurons in CeL (Haubensak et al., 2010; Li et al., 2013). Hierarchical cluster analysis were performed to classify the major cell type using 4 variables with nonuniform distribution (Figure 7c to 7f). Consistently, our cluster analysis of CeL neurons revealed two non-overlapping cell populations (Figure

7g), corresponding to LS and ES neurons, with a spike delay of 1769 ± 24 ms ($n = 46$) and 778 ± 86 ms ($n = 26$), respectively ($P < 0.001$, Wilcoxon rank-sum test). Notably, two distinct non-overlapping population can be revealed by the scatter-plot of spike delay v.s. ramp ratio (Figure 7h). The CeM is the main output station of the amygdala circuitry (Duvarci and Paré, 2014). We found that, in mouse amygdala, the CeM consisted of two major cell types (Figure 8a), based on their firing properties: low-threshold bursting (LTB) cells (76/147, 52%; Figure 8b) and ES cells (56/147, 38%; Figure 8c; Table 3). Unlike ES cells, LTB cells exhibited characteristic rebound APs after hyperpolarizing pulses (Figure 8a).

After cell type classification in the CeA (Figure 9a), we found ASIC currents with modest and similar densities in LS and ES neurons in the CeL (CeL-LS, 48 ± 13 pA/pF, $n = 12$; CeL-ES, 63 ± 15 pA/pF, $n = 6$; Figure 9b, 9c and 9f). Interestingly, in CeM, LTB neurons showed significantly larger ASIC current densities than those found in ES cells (CeM-LTB, 143 ± 23 pA/pF, $n = 14$; CeM-ES, 71 ± 12 pA/pF, $n = 9$; $P < 0.05$, Wilcoxon rank-sum test; Figure 9d to 9f). Thus, unlike the CeL, the CeM showed differential ASIC expression in different subpopulations of GABAergic neurons.

Modest expression of ASIC in ICMs

The ICM_{MV} and ICM_{MD} are clusters of GABAergic neurons between the BLA and CeA, receiving input from the BLA and sending projections to the CeL and CeM (Figure 2a) (Likhtik et al., 2008). On the other hand, the ICM_L is located on the dorsal–lateral side of the BLA, projecting inhibitory outputs to the BLA (Figure 2a) (Likhtik et al., 2008). We found that all ICM neurons showed similar electrophysiological properties (Table 4) and exhibited modest ASIC currents similar to CeL neurons (ICM_{MV}, 54 ± 8 pA/pF, n = 5; ICM_{MD}, 44 ± 9 pA/pF, n = 6; ICM_L, 54 ± 8 pA/pF, n = 5; Figure 10a to 10e).

In summary, the above functional mapping of ASIC current densities in diverse cell types of the amygdala network showed that ASICs were highly expressed in the major cell types of input (i.e. BLA) and output (i.e. CeM) regions of the amygdala (Figure 11).

ASICs in different types of amygdala neurons are functionally similar

ASIC subunit composition dictates gating properties (Askwith et al., 2004; Wemmie et al., 2006; Weng et al., 2010; Sherwood et al., 2011). We measured the desensitization τ of twelve types of neurons by fitting a mono-exponential function to the decay of ASIC currents (Figure 12a, top). Unlike the wide range of the ASIC current

densities among different cell types, the average desensitization τ_s of ASIC currents were very homogeneous among all types of neurons examined ($P = 0.52$, Kruskal-Wallis test; Figure 12a, bottom and 12b). Furthermore, the recovery time constants in both BLA-PNs ($\tau = 10s$) and CeM-LTB neurons ($\tau = 18s$) are similar to the recovery time course that previously found in hippocampal CA1 pyramidal neurons, which are expressing both ASIC1a and ASIC2 (Figure 12c to 12e; Weng et al., 2010). In keeping with this, the 20 s recovery ratios, which were measured by paired pulses with an interval of 20 s (Figure 12f, top), were also similar among the cell types investigated ($P = 0.65$, Kruskal-Wallis test; Figure 12f bottom and 12g).

Differential expression of ASICs selectively contributed to LTP in amygdala circuits

The functional significance of distinctly high ASIC expression in the main input (BLA-PNs) and output (CeM-LTB) amygdala neurons was further examined by studying synaptic plasticity in these neurons. A recent study shows that ASIC1a contributes to LTP at cortical inputs to BLA-PNs, and that alterations in proton-ASIC signaling modulate the magnitude of LTP at this synapse (Du et al., 2014). Since fear conditioning causes widespread plasticity at multiple synapses in amygdala circuits (Shin et al., 2006; Sah et al., 2008; Fourcaudot et al., 2009; Duvarci et al., 2011), we

investigated whether ASIC expression contributed to LTP at glutamatergic synapses onto various types of amygdala neurons. Using a standard HFS protocol, we compared LTP induction at glutamatergic synapses onto four distinct types of amygdala neurons (i.e., BLA-PN, CeM-LTB, CeM-ES, and CeL neurons) in brain slices from WT and *ASIC1a*^{-/-} (*Nestin*^{Cre/+}; *ASIC1a*^{fl/fl}) mice (Figure 13a to 13d, top). Consistent with a previous study (Du et al., 2014), we found that HFS evoked robust LTP ($211 \pm 25\%$; $n = 6$ cells, 4 animals; $P < 0.05$, Wilcoxon signed-rank test; Figure 13a, bottom) at cortex → BLA-PN synapses in WT littermates, but small LTP ($128 \pm 13\%$; $n = 7$ cells, 5 animals; $P = 0.15$, Wilcoxon signed-rank test; Figure 13a, bottom) in *ASIC1a*^{-/-} mutants. Interestingly, LTP evoked at BLA → CeM-LTB neuron synapses in WT neurons ($144 \pm 10\%$; $n = 10$ cells, 7 animals; $P < 0.05$, Wilcoxon signed-rank test; Figure 13b, bottom) was also significantly larger than that in *ASIC1a*^{-/-} neurons ($104 \pm 9\%$; $n = 10$ cells, 6 animals; $P = 0.92$, Wilcoxon signed-rank test; Figure 13b, bottom). In contrast, LTP evoked at BLA → CeM-ES neuron synapses in WT mice ($147 \pm 15\%$; $n = 9$ cells, 7 animals; $P < 0.05$, Wilcoxon signed-rank test; Figure 13c, bottom) was not significantly different from that in *ASIC1a*^{-/-} mice ($146 \pm 27\%$; $n = 9$ cells, 6 animals; $P = 0.08$, Wilcoxon signed-rank test; Figure 13c, bottom).

Glutamatergic inputs from the lateral IPB in the brainstem also exhibit LTP (López de Armentia and Sah, 2007; Watabe et al., 2013) and are required for conditioned fear learning and expression (Watabe et al., 2013). Similar to CeM-ES neurons, we found that LTP evoked at IPB → CeL neuron synapses in WT neurons ($140 \pm 7\%$; $n = 21$ cells, 16 animals; $P < 0.001$, Wilcoxon signed-rank test; Figure 13d, bottom) was similar to that in *ASIC1a*^{-/-} neurons ($132 \pm 9\%$; $n = 8$ cells, 5 animals; $P < 0.05$, Wilcoxon signed-rank test; Figure 13d, bottom).

Collectively, *ASIC1a* deletion caused a highly significant reduction in the magnitude of LTP in BLA-PNs and CeM-LTB neurons (Figure 13e), both of which exhibited the highest ASIC current density, whereas this deletion had little effect on LTP in CeM-ES and CeL neurons that expressed relatively low levels of ASICs. This suggests that the level of ASIC expression contributed to the extent of LTP induction.

In support of this idea, we found that the percentage of reduction in the LTP magnitude (Δ LTP%) in *ASIC1a*^{-/-} littermates, compared to WT mice, positively correlated with the ASIC current density observed in the postsynaptic neuron (Pearson's $R = 0.528$; $P < 0.001$, F-test; Figure 13f). Thus, the differential expression of ASICs among amygdala neurons contributed to LTP at both cortico-BLA and intra-amygdala glutamatergic synapses.

ASIC1a deletion in GABAergic neurons selectively impaired LTP at BLA-CeM neuron synapses

Next, we investigated whether LTP at cortex → BLA-PN synapses were normal if ASICs were deleted in GABAergic neurons only. By crossing *ASIC1a^{fl/fl}* mice with *GAD65-Cre* transgenic mice, we generated GABAergic neuron-specific conditional deletion of ASIC1a in their offspring. Indeed, normal ASIC currents were detected in BLA-PNs (Figure 14a, top), whereas ASIC currents were eliminated in CeM neurons (Figure 14b, top) in mice (*GAD65^{Cre/+}; ASIC1a^{fl/fl}*) with specific ASIC1a deletion in GABAergic neurons. In line with this finding, we also found that the application of HFS robustly induced LTP at cortex → BLA-PN synapses in mutant mice (*GAD65^{Cre/+}; ASIC1a^{fl/fl}*), which had the specific ASIC1a deletion in GABAergic neurons ($225 \pm 51\%$; $n = 9$ cells, 5 animals; $P < 0.01$, Wilcoxon signed-rank test; Figure 14a, bottom). On average, the magnitudes of LTP at cortex-BLA-PN synapses were similar in WT mice and mutants (Figure 14c). Finally, we tested whether selective deletion of ASIC1a in GABAergic cells, including amygdala output neurons, eliminated LTP in these cells. We found that HFS failed to induce significant LTP ($115 \pm 14\%$; $n = 9$ cells, 5 animals; $P = 0.30$, Wilcoxon signed-rank test; Figure 14b, bottom) at BLA-CeM-LTB neuron synapses in mutants (*GAD65^{Cre/+}; ASIC1a^{fl/fl}*), similar to no LTP in mice with pan-

neuronal ASIC1a deletion ($P = 0.60$, Wilcoxon rank-sum test; Figure 13e), but in contrast to marked LTP induction at the same synapse in WT mice (Figure 14d).

Deleting ASIC1a in BLA-PNs impaired conditioned fear learning.

The impairment of fear learning seen in ASIC1a-null mice could be prevented by specific transgenic expression of ASIC1a in the amygdala (Coryell et al., 2008). The finding that disrupting ASIC1a in mice resulted in deficits in LTP at cortex \rightarrow BLA-PN synapses has prompted the notion that ASIC-dependent LTP at the sensory inputs to the amygdala plays a critical role in conditioned fear learning (Du et al., 2014). Thus, we first measure the fear conditioning in the mice with pan-neuronal ASIC1a deletion or mice with selectively deletion of ASIC1a in BLA-PNs.

Pavlovian fear conditioning was used to test the role of ASICs in learned fear (LeDoux, 2000; Ehrlich et al., 2009). Mice were placed into the conditioning box (context A) and received five trials of tone-foot shock pairings. As illustrated (Figure 15a), an initially neutral, auditory pure-tone CS was paired with a noxious US (an aversive footshock). Consistent with previous studies (Wemmie et al., 2003; Coryell et al., 2008), during the training on day 1, we found that pan-neuronal ASIC1a deletion mice ($Nestin^{Cre/+}; ASIC1a^{fl/fl}$) showed decreased CS/US-induced freezing responses,

relative to WT littermates (Figure 15b), suggesting impaired fear learning in ASIC1a-deletion mice. On day 2, context- and cue-dependent fear memory was tested. We found that presenting either the training context or the cue (tone) elicited normal high-level freezing responses in WT mice (Contextual fear, $43.6 \pm 5.4\%$, $n = 10$; Figure 15c; Cued fear, $48.8 \pm 4.4\%$, $n = 16$; Figure 15d). However, mice with pan-neuronal ASIC1a deletion showed significantly lower freezing levels (Contextual fear, $12.8 \pm 4.6\%$, $n = 9$; $P < 0.001$, Wilcoxon rank-sum test; Figure 15c; Cued fear, $19.9 \pm 4.6\%$, $n = 9$; $P < 0.001$, Wilcoxon rank-sum test; Figure 15d).

Next, we tested the behavioral impact of selective deletion of ASIC1a in glutamatergic PNs of the BLA, using the Cre/loxP system. We found that bilaterally injecting an adeno-associated viral vector serotype 8 (AAV8), encoding GFP-Cre under the control of the CaMKII α promoter (AAV8-CaMKII α -GFP-Cre), into the BLA of *ASIC1a*^{fl/fl} mice specifically eliminated ASIC currents in virus-transfected BLA-PNs, but not in non-transfected neurons (Figure 16a) or neurons transduced with the fluorophore alone (Figure 16b). Moreover, *ASIC1a*^{fl/fl} mice that received the viral vector encoding GFP-Cre in the BLA exhibited lower freezing levels than mice injected with a viral vector encoding GFP alone during conditioning (Figure 16c). During both contextual and cued recall test, mice injected with a viral vector encoding GFP alone

had normal high-level freezing responses (Contextual fear, $46.1 \pm 4.6\%$, $n = 8$; Figure 16d; Cued fear, $60.0 \pm 6.8\%$, $n = 8$; Figure 16e). Similar to pan-neuronal deletion of ASIC1a, mice with selective deletion of ASIC1a in BLA-PNs showed significantly lower freezing level than control mice (Contextual fear, $16.6 \pm 4.5\%$, $n = 9$; $P < 0.001$, Wilcoxon rank-sum test; Figure 16d; Cued fear, $27.4 \pm 5.5\%$, $n = 9$; $P < 0.001$, Wilcoxon rank-sum test; Figure 16e). These results supports the important role of ASICs in the BLA-PNs.

Deleting ASIC1a in GABAergic neurons impaired conditioned fear learning.

Finally, in light of the present finding of ASIC-dependent LTP in the amygdala output neurons, we further examined whether deleting ASIC1a in GABAergic neurons also affected conditioned fear behavior. Using mice with a specific deletion of ASIC1a in GABAergic neurons ($GAD65^{Cre/+}; ASIC1a^{fl/fl}$), we next test the behavioral effects of ASIC1a deletion in GABAergic neurons only. On day 1, we found that mice with specific deletion of ASIC1a in GABAergic neurons showed lower freezing responses than WT mice during training on day 1 (Figure 17a). On day 2, we found that freezing level of mice with specific deletion of ASIC1a in GABAergic neurons is significantly reduced in both contextual and cued fear test (Contextual fear, $10.2 \pm 2.3\%$, $n = 10$; P

< 0.001, Wilcoxon rank-sum test; Figure 17b; Cued fear, $17.0 \pm 2.3\%$, $n = 16$; $P < 0.001$, Wilcoxon rank-sum test; Figure 17c). Interestingly, mice with specific ASIC1a deletion in GABAergic neurons also exhibited impaired learning behavior similar to that found in pan-neuronal ASIC1a-deletion mice (Contextual fear, $P = 0.55$, Wilcoxon rank-sum test; Cued fear, $P = 0.59$, Wilcoxon rank-sum test). In summary, these results indicate that ASIC1a expression in GABAergic neurons was as important as ASIC1a expression in glutamatergic neurons in supporting conditioned fear behavior.



Conclusion

The amygdala consists of various cell-types in the distinct nuclei. To understand the role of ASICs in fear learning and memory, we measured the functional expression level of ASICs in various types of amygdala neurons. Using *ASIC1a*^{-/-} and *ASIC2*^{-/-} mice, we showed that ASIC1a and ASIC2 are co-expressed in the amygdala neurons. Moreover, the expression level of ASICs is highly variable and cell type-specific, but the subunit compositions of ASICs are very similar throughout the amygdala network. In support of the notion that ASIC is a synaptic modulator, we found that the extent of LTP correlated positively with the ASIC current density in the postsynaptic neuron. ASIC is not only play a role in the cortex → BLA input synapses, but also important for the synaptic plasticity at BLA → CeM-LTB neuron synapses. Importantly, ASIC1a deletion in GABAergic neurons only eliminated LTP of intra-amygdala glutamatergic synapses onto CeM output neurons and reduced both contextual and cued fear memory to the same extent as that found for ASIC1a deletion in all neurons or selectively in BLA glutamatergic PNs. Thus, fear learning requires ASIC-dependent LTP at multiple amygdala synapses, including both cortico-BLA input synapses, as well as intra-amygdala synapses on output neurons.

Chapter 3

Discussion

Significance of this study

Amygdala serves as the key brain structure of the neuronal circuitry underlying fear learning (Ehrlich et al., 2009; Duvarci and Paré, 2014). Accumulating evidences indicate that anxiety and panic disorder result from abnormal regulation of amygdala network (Duvarci and Paré, 2014; Smoller et al., 2014). Moreover, panic disorder and amygdala dysfunction are associated with genetic variants of ASIC1a ortholog gene, *ACCN2*, in human (Smoller et al., 2014). Multiple evidences indicate that fear conditioning requires activation of ASICs in the amygdala (Wemmie et al., 2003; Coryell et al., 2008; Ziemann et al., 2009). To reveal the functional role of ASICs in fear learning and memory, it is fundamentally important to characterize the expression pattern and properties of ASICs in the fear circuitry. In this study, to our knowledge, we made the first detailed functional mapping of ASICs in the amygdala networks. Moreover, we further characterized ASIC function in the amygdala at synaptic, and

behavioral levels. We found that ASICs are highly expressed in the primary input (i.e. BLA) and output station (i.e. CeM) of fear circuitry and show region specific and cell-type specific expression pattern in the amygdala network. Most importantly, when ASIC1a is selectively deleted in GABAergic cells, including CeM output neurons, in mice, LTP in these cells and fear learning are reduced to the same extent as that found in mice with selectively deletion of ASIC1a in BLA glutamatergic neurons. Thus, ASIC-dependent LTP at intra-amygdala synapses on output neurons is as important as ASIC-dependent LTP at cortico-BLA input synapses in the fear learning and memory.

ASIC1a, 2a and 2b are coexpressed in amygdala neurons

The gating properties of ASICs described here including desensitization and recovery time course (Figure 12) are similar to those of CA1 pyramidal neurons, which contain a mixture of homomeric ASIC1a, heteromeric ASIC1a/2a, and heteromeric ASIC1a/2b channels (Baron et al., 2002; Weng et al., 2010). PcTX1 is known to inhibit ASIC1a homomers and ASIC1a/2b heteromers, but not ASIC1a/2a heteromers (Sherwood et al., 2011). Therefore, the great majority (approximately 80%) of ASICs in amygdala neurons is likely mediated by ASIC1a/2a heteromers. Conversely, the PcTX1-sensitive component (approximately 20%) is mediated by ASIC1a homomers

and/or ASIC1a/2b heteromers. Notably, the current (putatively mediated by ASIC1a homomers) in *ASIC2^{-/-}* mice, which is approximately 20% of the total current in WT mice, exhibits a rapid cumulative reduction in responses to successive applications of proton. Since only ASIC1a homomer has fast cumulative desensitization τ (Chen et al., 2007), we speculate that PcTX1-sensitive component is primarily mediated by ASIC1a homomers. The difference in ASIC current densities in various cell types reflects the variation in the expression of ASIC subunits. In our study, since no difference in gating properties was found in ASIC currents recorded from all cell types (Figure 12), the differential expression of ASICs in each cell type may involve the coordinated regulation of ASIC subunit expression, without altering the relative contribution by ASIC1a homomer, and ASIC1a/2b and ASIC1a/2a heteromers.

ASIC is important in primary input and output station of amygdala circuitry

With a detail measurement of ASIC currents in various cell types, we found that the major cell types of primary input (i.e. BLA) and output (i.e. CeM) station of fear circuitry (Figure 11), which are critical for acquisition and expression of learned fear, have the highest expression level of ASICs in the amygdala. These results consistence with the behavioral observations in the previous studies that ablation of ASICs leads to

deficits in fear conditioning (Wemmie et al., 2003; Coryell et al., 2008; Price et al., 2014). On the other hand, CeM output neurons can be bidirectionally modulated by ICMs and CeL neurons (Figure 1b and 1c). Some groups of neurons in ICMs and CeL can directly inhibit the CeM output neurons, other groups can promote the activity of CeM neurons by disinhibition (Figure 1b and 1c). However, ASICs are modestly expressed in all types of ICMs and CeL neurons (Figure 11). These results suggest that ASIC might play a role in the BLA and CeM but not in the ICMs and CeL.

Postsynaptic ASIC is a positive regulator of synaptic plasticity

Two recent studies show that ASICs participate in synaptic transmission in the amygdala and nucleus accumbens where they contribute to approximately 5% of excitatory postsynaptic currents (Du et al., 2014; Kreple et al., 2014). We speculate an important role of proton-ASIC signaling during intense presynaptic stimulation. During basal transmission, synaptic pH drop is rapidly buffered by a variety of homeostatic mechanisms (Chesler and Kaila, 1992). Massive extracellular pH reductions may occur during intense activity such as fear conditioning. The lower pH can generate larger ASIC currents, thereby boosting NMDA receptor function (Wemmie et al., 2002). These effects could explain the involvement of protons and the requirement of ASICs for LTP induced by HFS. In this scenario, the strength of proton-ASIC signaling should

be critical in determining the relative contribution of ASICs to learning, memory, and synaptic plasticity. Indeed, several lines of evidence support this view. First, ASIC1a and ASIC2 expression in the hippocampus is relatively low, compared to other brain regions (Wemmie et al., 2003; Price et al., 2014). Consistent with this, *ASIC1a*^{-/-}, *ASIC2*^{-/-}, and *ASIC1a/2*^{-/-} mice display normal spatial learning and memory (Wu et al., 2013; Price et al., 2014). Second, ASIC currents during synaptic transmission are not detected in the hippocampus. In keeping with this, LTP at CA3-CA1 synapses can be readily induced in *ASIC1a*^{-/-} mice (Wu et al., 2013). Third, the observed effects of ASICs on synaptic plasticity, learning, and behavior are found in the amygdala and nucleus accumbens, the brain regions where ASICs are highly enriched (Du et al., 2014; Kreple et al., 2014). Fourth, increasing or decreasing pH buffering capacity can bidirectionally modulate the magnitude of LTP at cortex → BLA-PN synapses (Du et al., 2014). Finally, in our study, the reduction in the magnitude of LTP at different glutamatergic synapses in *ASIC1a*^{-/-} mice, relative to WT controls, correlates positively with the abundance of ASICs in postsynaptic neurons (Figure 13). Collectively, our study also supports the view that postsynaptic ASIC is a positive regulator of associative fear learning and memory at both the synaptic and behavioral levels. Such knowledge could be of importance for future drug discovery and development.

ASIC-dependent LTP in multiple glutamatergic synapse are required for fear conditioning

It is intriguing to note that mice with ASIC1a disruption in GABAergic neurons (GAD65^{Cre/+}; ASIC1a^{fl/fl}) show a similar extent of fear learning/memory deficit as mice with pan-neuronal deletion of ASIC1a (Nestin^{Cre/+}; ASIC1a^{fl/fl}). The CeM is the final output station projecting to the brainstem areas (Viviani et al., 2011), which are responsible for freezing expression. The selective disruption of synaptic plasticity at the BLA → CeM-LTB synapses, but not cortex → BLA-PN synapses, in mice with selectively disruption of ASIC1a in GABAergic neurons indicates a central role of the CeM in fear acquisition and expression. Finally, we speculate that similar changes in LTP induction can be observed in cortex → BLA-PN or BLA → CeM-LTB pathway induced by selective deletion of ASIC1a in glutamatergic neurons using the AAV-Cre/loxP system. However, if it is not the case, it implies that deletion of ASICs during early embryonic stages may disrupt synapse formation or alter the synaptic function during the development. If restoring ASIC1a with AAV-ASIC1a can rescues LTP in these two pathways in ASIC1a-null mice, it can exclude the essential role of ASIC during development.

ASICs in subcellular level

Our recent study shows differential expression of ASICs in different cell types within hippocampal networks (Weng et al., 2010). Somatic ASIC current density of oriens lacunosum-moleculare (O-LM) cells in the CA1 region, a classical type of dendrite-targeting IN, is six times greater than that of fast-spiking basket cells (BCs) in the dentate gyrus, a major class of soma-targeting IN. Similarly, ASIC currents in dendrites of O-LM cells evoked by local acid puffing are approximately six-fold greater than those in BC dendrites at remote distances (up to 100 μm) from the soma (Weng et al., 2010). Nevertheless, there is a general concern whether somatic ASICs are equally representative of those in the synaptic membrane. However, unlike cortex and hippocampus, amygdala is lack of lamina structure and orientation (Figure 2), acid-induced dendritic currents cannot be accurately measured in the amygdala. In this study, a detailed characterization of ASICs was made from patches excised from somata rather than dendrites. Therefore, it is important to be aware of this potential pitfall in the interpretation of the correlation between the extent of LTP and the ASIC current density in the postsynaptic neurons. Finally, people should keep in mind that the extent of ASIC-dependent LTP might be sensitive to the patterns of induction paradigms used at synapses. In this study, we used the LTP induction protocol for each synapse type according to previous studies (see Materials and Methods in Chapter 3).

A recent study finds that disrupting ASIC1a leads to an increase in spine density and changes in glutamate receptor function in nucleus accumbens, although the underlying mechanisms remain unknown (Kreple et al., 2014). Thus, it is worth to note that our study did not exclude the possibility that ASICs are involved in regulation of synapse structure and function in the amygdala neurons. Further experiments are needed to investigate whether ASIC is required for LTP in a cell-autonomous fashion.

The possible role of ASICs in the BLA-INs

Various GABAergic INs in the BLA play important role in controlling fear learning and memory (Ehrlich et al., 2009; Wolff et al., 2014). Thus, we cannot exclude the possibility that ASIC1a deletion in GABAergic INs in *GAD65^{Cre/+}; ASIC1a^{fl/fl}* mice causes abnormal inhibitory control in the BLA, given that ASIC expression levels are high in most BLA-IN subtypes. The BLA has two major types of INs, PVINs and SOMINs, which are playing different roles in the fear conditioning. During auditory fear conditioning, the activation of PVINs promote the excitability of PNs by inhibiting SOMINs, thereby facilitate the auditory responses and CS-US associations (Wolff et al., 2014). However, both PVINs and SOMINs are inhibited during an aversive footshock. In this study, we found that FSINs, the major population of PVINs (Song et

al., 2013), have the lowest expression level of ASICs in the amygdala. In contrast, ASIC is highly expressed in the non-FSINs (Figure 11), including SOMINs. The activation of ASICs in the SOMINs can inhibit the PNs and reduce the fear response. But recent study shows that SOMINs are strongly inhibited during both auditory tone and aversive footshock in the fear conditioning (Wolff et al., 2014). The high expression level of ASICs fail to promote the activity of SOMIN during fear conditioning. It suggests that expression of ASICs in the SOMINs might not play a role in the fear conditioning. However, the expression of ASIC in the SOMINs may also participate in amygdala-dependent behaviors other than fear conditioning, e.g. innate fear and fear extinction.

In addition, there are other types of non-FSINs in the amygdala, such as vasoactive intestinal polypeptide-expressing INs (VIPINs) and cholecystokinin-expressing INs (CCKINs) (Jasnow et al., 2009; Mascagni and McDonald, 2003). Previous study shows that CCKINs can inhibit PNs with perisomatic inhibitory projection (Katona et al., 2001). In contrast, the VIPIN plays disinhibitory role by suppressing SOMINs and PVINs (Pi et al., 2013). But unlike PVIN and SOMIN, the neuronal activity and contribution of CCKINs and VIPINs in the fear conditioning is not very clear. Overall, the functional role of ASICs in the BLA-INs is another important question remained to be answered.

The possible role of ASICs in fear extinction

Although we found that the abundant expression of ASICs in both GABAergic neurons and glutamatergic PNs in the amygdala is critical for fear conditioning, the role of ASICs in the fear extinction remains unknown. As the center of fear learning circuitry, amygdala is also critical for fear extinction (Paré and Duvarci, 2012; Ehrlich et al., 2009). GABAergic projection from ICMs and CeL suppress the output of CeM and reduce the fear response (Amano et al., 2010; Haubensak et al., 2010; Paré and Duvarci, 2012). Selective lesion of ICMs (Likhtik et al., 2008) or inhibition the input to the ICMs by pharmacological approach (Jüngling et al., 2008) can reduce the extinction of learned fear. Activation of output neuron in the CeL (Haubensak et al., 2010; Ciocchi et al., 2010) can reduce the fear response. Moreover, in the BLA, silencing of BLA-PNs during fear extinction is caused by increasing of perisomatic inhibition from PVINs (Trouche et al., 2013), which are mostly FSINs (Woodruff et al., 2007; Song et al., 2013). Interestingly, we found that ASICs are modestly expressed in the ICMs, CeL and BLA-FSINs.

However, recent studies show that a subpopulation of “extinction cells” (~15%; Herry et al., 2008; Popescu et al., 2011) are exist in the BLA-PNs, which can collateral

inhibit “conditioning cells” during fear extinction. The high expression level of ASICs in the “extinction cells” might play a role in fear extinction. Further investigation are required to understand the contribution of ASICs in the fear extinction.

ASICs may have different role in the amygdala during seizure

Activation of ASICs by acidosis during seizures has been suggested to enhance inhibition through GABAergic inhibitory INs in the cortex and hippocampus (Ziemann et al., 2008). Moreover, disrupting ASIC1a in mice increased the severity of chemoconvulsant-induced seizure in the hippocampus (Ziemann et al., 2008). Consistent with this, in the hippocampus, ASICs are highly expressed in the GABAergic INs but less expressed in glutamatergic PNs (Weng et al., 2010). The amygdala also plays a critical role in temporal lobe epilepsy (Schramm, 2008; Graebenitz et al., 2011; Lévesque and Avoli, 2013). However, in contrast to the hippocampus or cortex, glutamatergic BLA-PNs express the highest ASIC current density. As a result, reductions of extracellular pH during seizure can increase the activity of both glutamatergic PNs and several subtypes of GABAergic INs in the BLA through the activation of ASICs (Pidoplichko et al., 2014). Thus, during seizure, the role of ASICs in the amygdala might be different from that in the hippocampus.

Consistent with this possibility, the role of ASICs in the nucleus accumbens is in apparent contrast with the previously observed effects of ASICs in promoting learning and memory in amygdala-dependent learning and synaptic plasticity (Kreple et al., 2014). Selective disrupting ASIC1a there increased cocaine-evoked plasticity and increased cocaine-conditioned place preference, a model of drug reward-associated learning and memory (Kreple et al., 2014).

Functional role of CeM neurons

The high level of ASIC expression in the CeM output neurons of the fear circuitry is in accordance with the behavioral observation that ASIC1a deletion leads to deficits in fear acquisition and expression. In terms of fear expression, at least two types of CeM neurons project to two distinct brainstem sites: the periaqueductal gray and dorsal vagal complex (Viviani et al., 2011). With respect to brainstem-projecting neurons, whether there is a correspondence between the cell type (i.e., LTB versus ES) and their brainstem site remains unknown. On the other hand, information transfer from the BLA to the CeM is flexibly gated, depending on the specific pattern of environmental cues confronting the animal (Paré et al., 2003). It is thought that the CeL and ICMs fulfill this function, as they receive glutamatergic inputs from the BLA and send GABAergic

projections to the CeM (Duvarci and Paré, 2014). As described above, ASICs are modestly expressed in CeL and ICM neurons. The role of ASICs in these neurons and their relative contribution to the acquisition of fear conditioning and expression of conditioned fear require further studies, for which cell type-specific gene disruption, as demonstrated here, would prove useful.

Ample evidences indicate that the output neurons of fear circuitry in CeM are as important as BLA neurons in acquisition and expression of learned fear (Ehrlich et al., 2009; Zimmerman et al., 2007). The activity of CeM neurons are increased during fear conditioning and recall tests, and are reduced after the extinction of fear memory (Duvarci et al., 2011). Lesion of CeM or reducing the activity of CeM neurons by pharmacological approach leads to impairment of fear learning and memory (Goosens and Maren, 2001; Ciochi et al., 2010). Injection of NMDA receptor antagonist into CeA, which consists of CeL and CeM, also reduces the acquisition of fear memory (Goosens and Maren, 2003). However, whether LTP at intra-amygdala synapses onto CeM output neurons is important for fear conditioning remains unclear. Importantly, in this study, we found that fear learning and memory were impaired when LTP at intra-amygdala synapses onto output neurons were specifically eliminated without changing of the LTP at cortico-amygdala synapses and LTP at IPB-CeL synapses by ASIC1a

deletion in GABAergic neurons in conditional knockout mice ($GAD^{Cre/+}; ASIC1a^{fl/fl}$).

In conclusion, these results provide another evidence that LTP at intra-amygdala synapses onto output CeM neurons is as important as cortico-amygdala synapses in fear learning and memory.



Figures

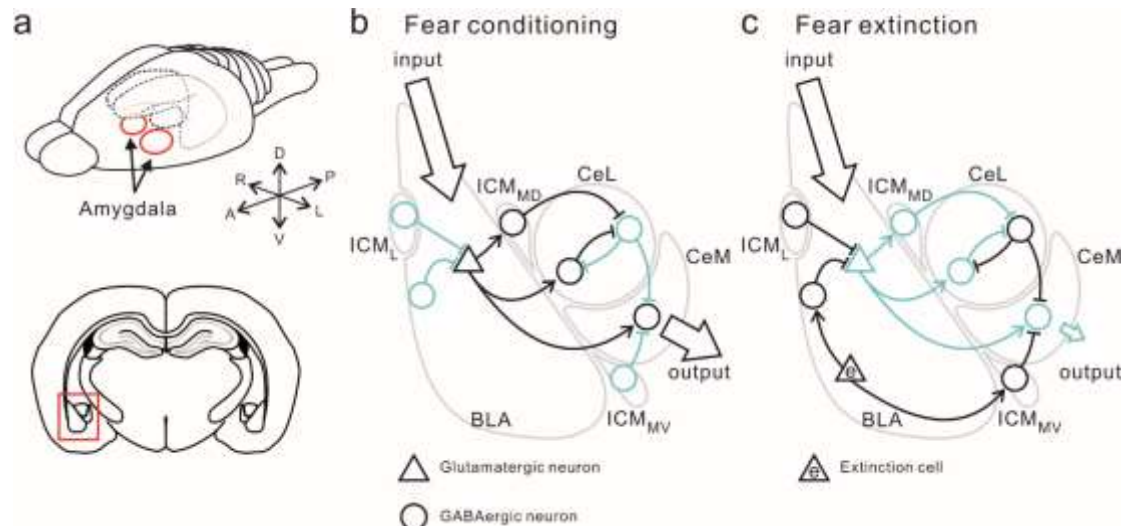


Figure 1 | Fear circuitry within the amygdala

(a) Top, schematic drawing shows the location of amygdala in the brain. The dash line and red line indicates the hippocampus structure and the amygdala. Bottom, the location of amygdala, indicated by red square, in the coronal brain section. Axis: L, left; R, right; A, anterior; P, posterior; D, dorsal; V, ventral.

(b) Schematic diagram of fear conditioning circuitry in the amygdala. Light blue indicates the suppressed neurons during fear conditioning. Triangle, glutamatergic PNs; Circle, GABAergic neurons.

(c) Schematic diagram of fear extinction circuitry in the amygdala. Light blue indicates the suppressed neurons and pathway during fear extinction. Triangle, glutamatergic PNs; Circle, GABAergic neurons. Triangle with “e”, extinction cell.



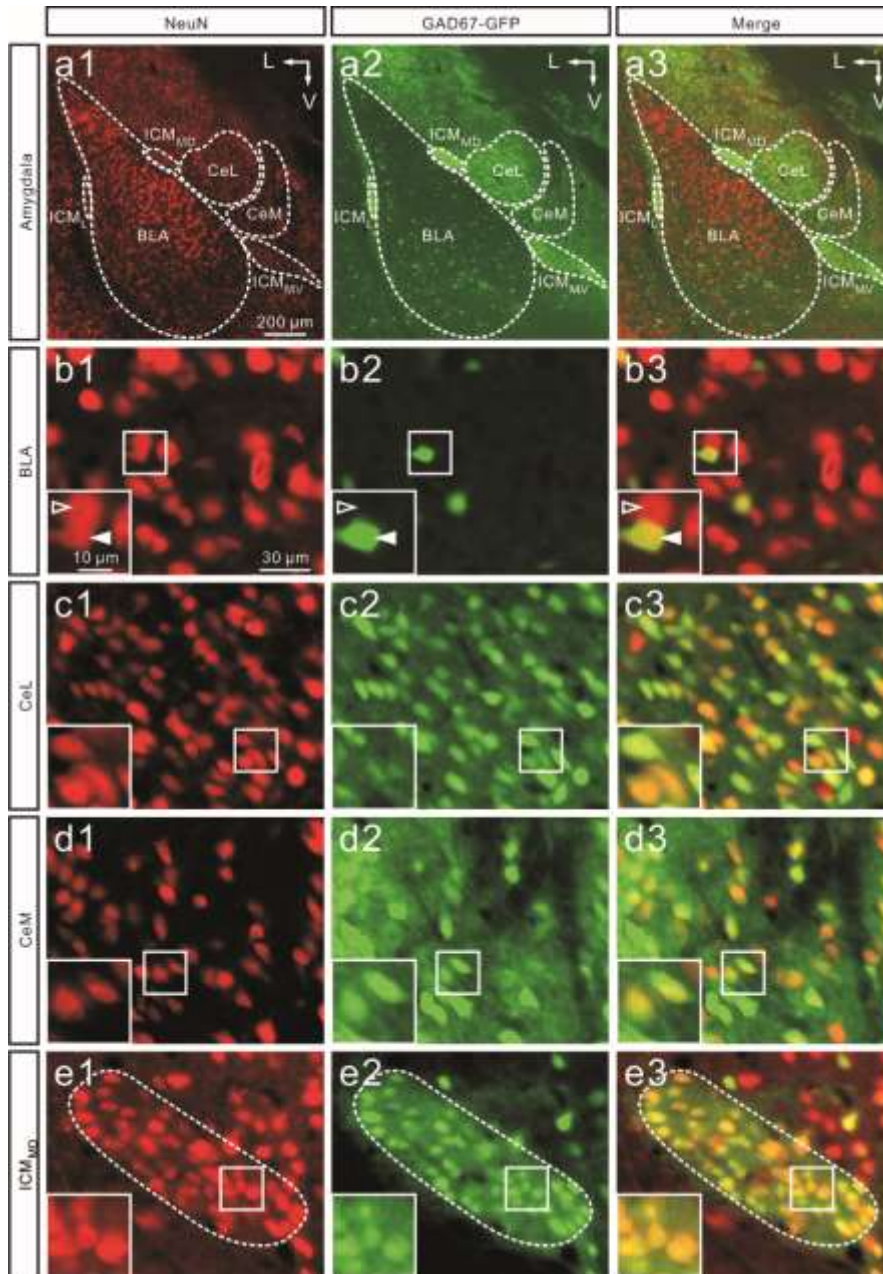


Figure 2 | GAD67-GFP labeled cells in the amygdala complex

(a) A coronal brain section from a GAD67-GFP KI mouse. (a1) Immunostaining of NeuN of the amygdala. The borders of BLA, CeL, CeM and ICM clusters are outlined.

(a2) GAD67-GFP labelled cells in the same slice. Green spots indicate endogenous GFP epifluorescence of GABAergic cell bodies. (a3) the merged image. BLA, basolateral amygdala; CeL/CeM, lateral/medial divisions of the central amygdala; ICM_{MD}, medial-dorsal intercalated cell mass; ICM_{MV}, medial-ventral ICM; ICM_L, lateral ICM. Axis: L, lateral; V, ventral. Scale bar in (a1) applies to (a2) and (a3).

(b) NeuN- and GFP-labelled BLA (b1 and b2) and merged images (b3). Note that GFP⁺ cells are sparsely scattered in the BLA, which is a cortex-like nucleus. The insets show enlargements of the boxed areas; filled and open arrowheads indicate GFP⁺ and GFP⁻ cells, respectively. Scale bars in (b1) applies to all Figures in (b2) and (b3).

(c - e) NeuN- and GFP-labelled CeL (c1 and c2), CeM (d1 and d2) and ICM_{MD} (e1 and e2) cells and merged images (c3, d3 and e3). Note that GFP⁺ cells are the major cell types in the CeL, CeM and ICM_{MD} (c3, d3 and e3). The insets show enlargements of the boxed areas; filled and open arrowheads indicate GFP⁺ and GFP⁻ cells, respectively. Scale bars in (b1) applies to all Figures in (c) to (e).

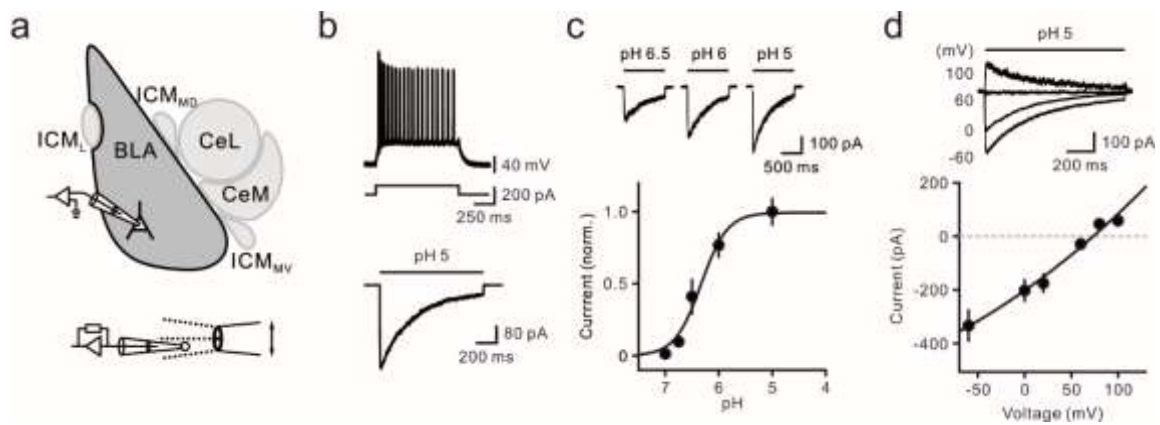


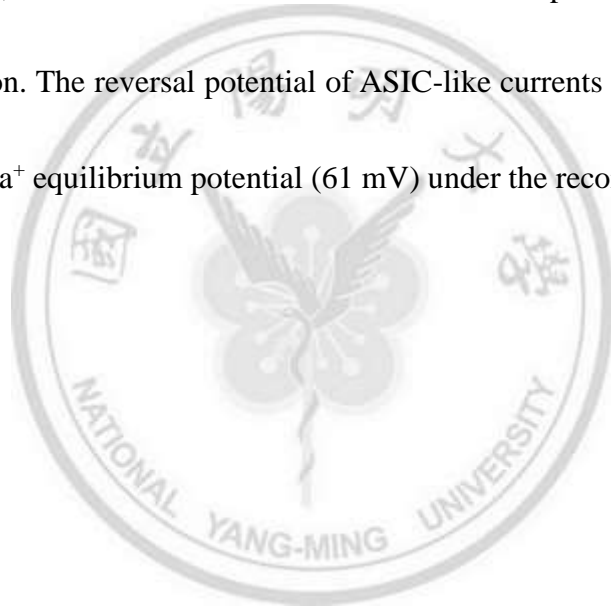
Figure 3 | ASIC currents in mouse amygdala neurons

(a) Scheme of the whole-cell recording configuration (top) and fast application of H^+ to a nucleated patch recording (bottom). After measured the electrophysiology properties of neuron (top), ASIC currents of the same neuron were measured by nucleated patch recording and fast application system (bottom)

(b) Top, firing pattern of a BLA-PN and the current protocol. Bottom, schematic of fast application of H^+ to a nucleated patch and averaged ASIC current (from seven trials) recorded from the same cell.

(c) Top traces, ASIC currents recorded from BLA-PNs evoked by different pH reductions. Bottom, normalized peak amplitude of ASIC current plotted against pH value. The curve depicts the single Hill equation (half-maximal pH 6.3, Hill coefficient 1.8) fitted to the data points. Points represent mean values from four to 20 experiments.

(d) Top traces, ASIC currents recorded from a BLA-PN at different membrane potentials. Bottom, the I - V curve of ASIC currents. Data points are fitted with a polynomial function. The reversal potential of ASIC-like currents (67.8 ± 5.2 mV, $n = 6$) is close to the Na^+ equilibrium potential (61 mV) under the recording condition.



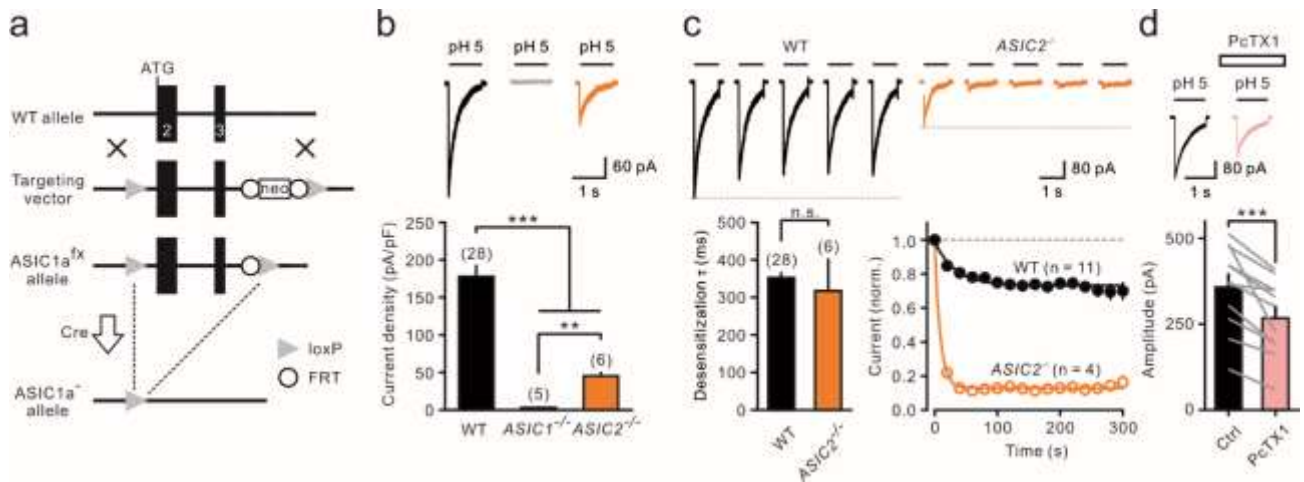


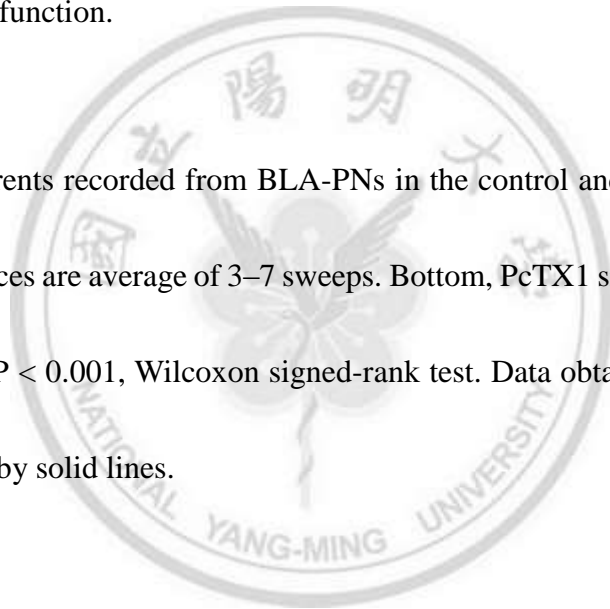
Figure 4 | ASIC currents in mouse amygdala neurons were mediated by ASIC1a and ASIC2 subunits.

(a) A schematic diagram of the gene targeting strategy to knockout ASIC1a gene by deletion of exons 2 and 3 using the Cre/loxP recombination system.

(b) Top, example traces of ASIC currents recorded from BLA-PNs of WT, ASIC1a^{-/-} and ASIC2^{-/-} mice. Bottom, bar graph of the average current density. Note that ASIC currents are completely abolished in the ASIC1a^{-/-} mice and significantly reduced in the ASIC2^{-/-} mice. **P < 0.01; ***P < 0.001, Wilcoxon rank-sum test.

(c) Top, examples of ASIC currents recorded from BLA-PNs of WT and *ASIC2*^{-/-} mice; currents were evoked by repetitive 1 s pulses (from pH 7.4 to 5) at 0.05 Hz. Only the first five traces are shown. Bottom, bar graph of the average desensitization τ of ASIC currents (left) and time course of cumulative reduction in the current amplitude during repeated stimulation (right). Current amplitudes were normalized to the first amplitude and were plotted against the time of each pulse. Continuous lines represent fits to a single exponential function.

(d) Top, ASIC currents recorded from BLA-PNs in the control and in the presence of 30 nM PcTX1. Traces are average of 3–7 sweeps. Bottom, PcTX1 significantly reduced ASIC currents. *** $P < 0.001$, Wilcoxon signed-rank test. Data obtained from the same cell are connected by solid lines.



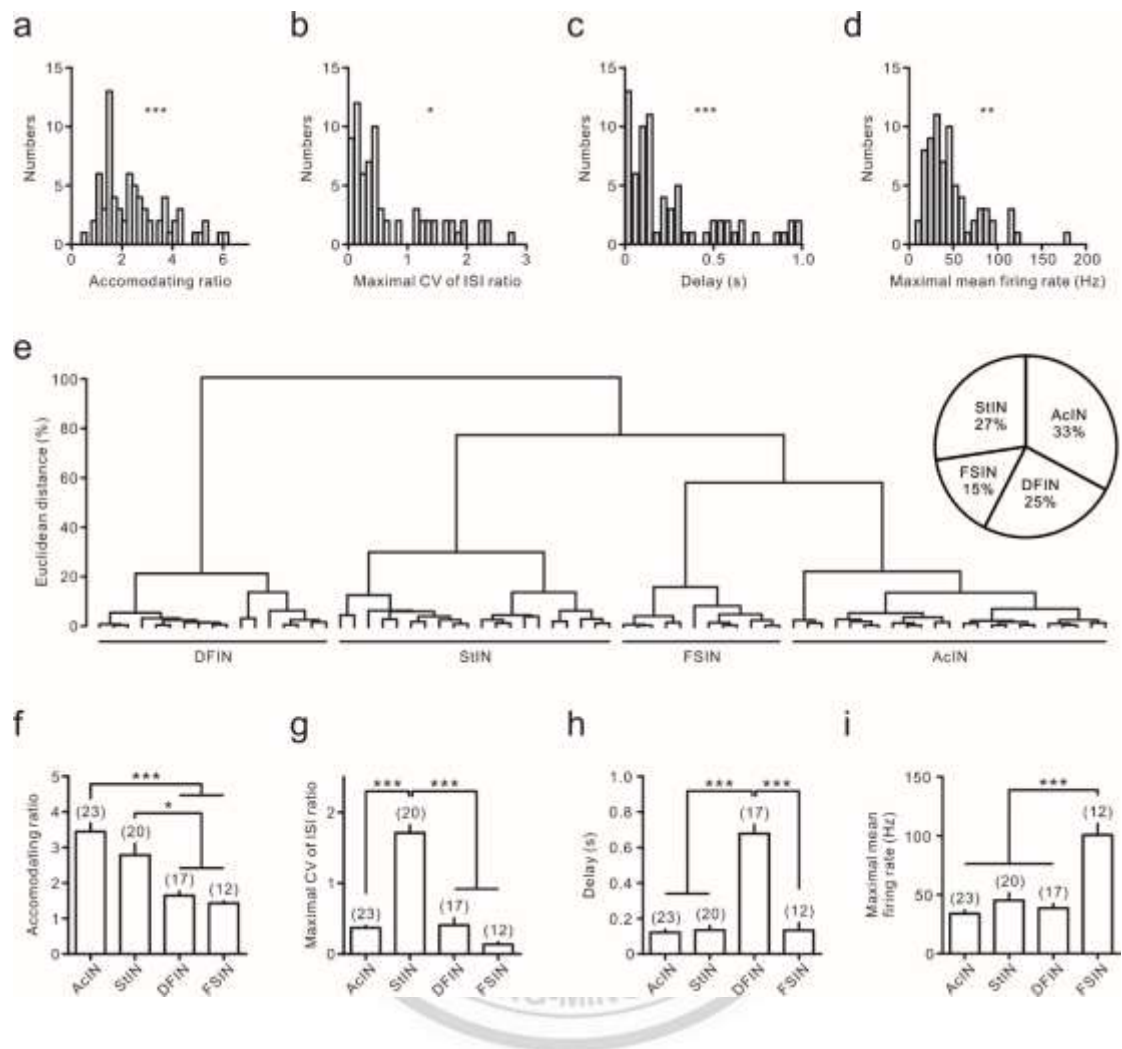


Figure 5 | Classification of GABAergic INs in the BLA

(a) – (d), Histograms of accommodating ratios, maximal CVs of ISI ratios, delays of AP and maximal mean firing rates from GFP⁺ cells in the BLA. The D’Agostino and

Pearson omnibus normality test demonstrates that the properties presented are not unimodally distributed. Asterisks indicate significant deviation from a normal distribution (*P < 0.05, **P < 0.01, ***P < 0.001).

(e) Hierarchical cluster analysis of GABAergic INs performed with electrophysiological parameters shown in a-d as the parameters for classification. The x axis of the dendrogram represents the individual cells, and the y axis represents the rescaled distance (squared Euclidean) between groups. Distinct subtypes of INs are marked with bars below the dendrogram. Inset, pie chart shows proportion of each BLA-IN subtype.

(f) – (i), Bar graphs comparing accommodating ratios, maximal CVs of ISI ratios, delays of AP and maximal firing rates among different IN subtypes (*P < 0.05, ***P < 0.001, Wilcoxon rank-sum test after Kruskal-Wallis test).

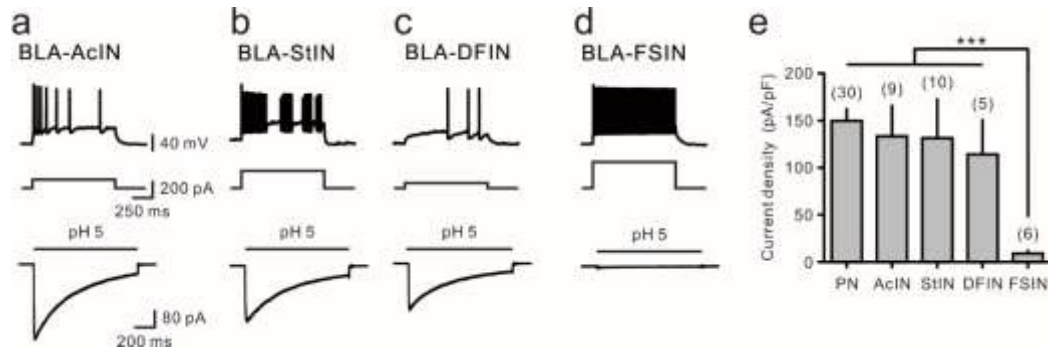


Figure 6 | Mapping of ASIC expression in different types of BLA neurons.

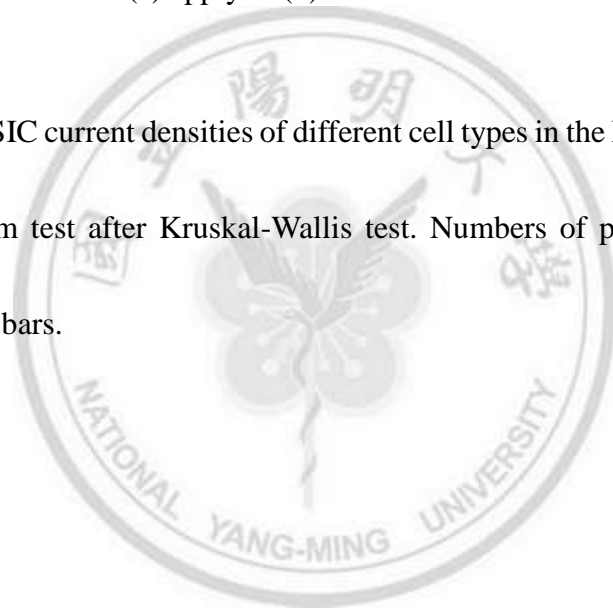
(a) Top, an example of accommodating firing pattern recorded from an AcIN with a current step injection. Bottom, averaged ASIC currents from 13 trials recorded from the same cells.

(b) Top, an example of stuttering firing pattern recorded from a StIN with a large current step injection. Bottom, averaged ASIC currents from 15 trials recorded from the same cells. Scale bars in (a) apply to (b).

(c) Top, an example of delayed firing pattern recorded from a DFIN with a small current step injection. Bottom, averaged ASIC currents from 12 trials recorded from the same cells. Scale bars in (a) apply to (c).

(d) Top, high frequency action potentials can be induced from a FSIN with a large current step injection. Bottom, averaged ASIC currents from 14 trials recorded from the same cells. Scale bars in (a) apply to (d).

(e) Summary of ASIC current densities of different cell types in the BLA. *** $P < 0.001$; Wilcoxon rank-sum test after Kruskal-Wallis test. Numbers of patches are given in parentheses above bars.



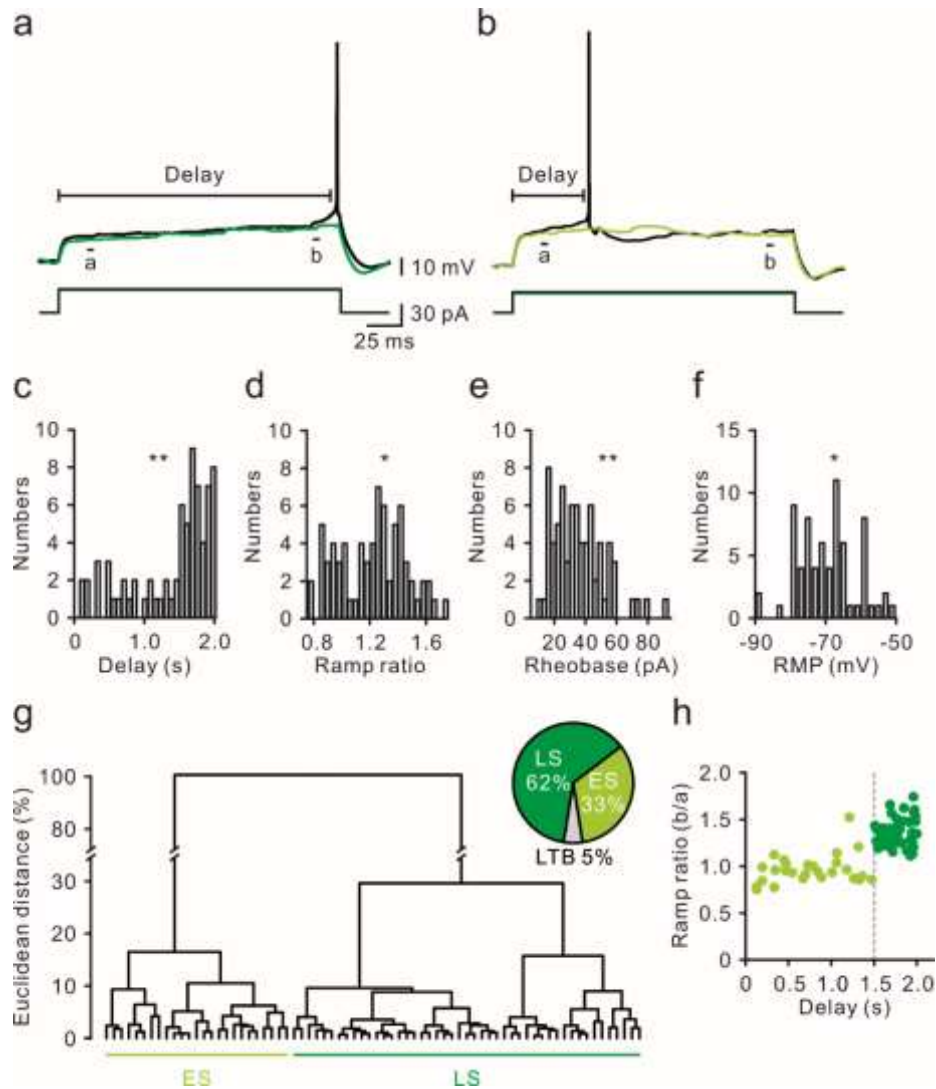


Figure 7 | Classification of GABAergic neurons in the CeL

(a) – (b), Membrane responses to supra- (black) and sub-threshold (dark and light green) current pulse injections recorded from a representative LS (a) and ES cell (b). Note the slow depolarizing ramp of the membrane response in the LS cell but not in the ES cell.

Bars a and b indicate how the average membrane potentials were measured for the calculation of ramp ratio (b/a).

(c) – (f), Histograms of spike delays, ramp ratios, rheobases and resting membrane potentials (RMPs) from non-LTB cells. Asterisks indicate significant deviation from a normal distribution (*P < 0.05, **P < 0.01, D’Agostino and Pearson omnibus normality test).

(g) Dendrogram of non-LTB neurons. The y axis represents the normalized Euclidean distance. Color codes indicate cell classification based on spike delay; cells with spike delay > 1.5 s were dark green otherwise light green. Inset, pie chart shows distinct populations in the CeL. Dark and light green areas denote the major cell populations, LS and ES neurons. Gray area depicts a small subset of LTB neurons.

(h) Scatter-plot of spike delay vs. ramp ratio. The dotted line indicates the arbitrary cutoff value (spike delay of 1.5 s) that best separates the two populations.

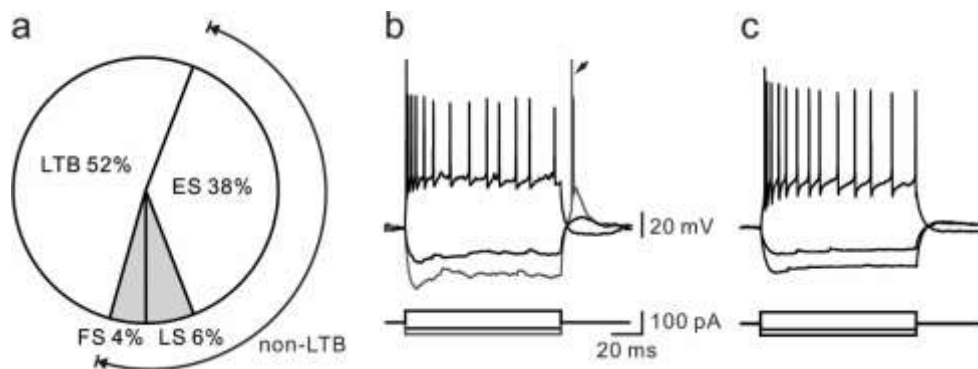


Figure 8 | Two distinct major cell types in the CeM

(a) Pie chart showing distinct populations in the CeM. White areas denote the major cell populations, LTB and ES neurons. Gray area depicts a small subset of FS and LS neurons.

(b) Membrane responses to different current pulses recorded from the representative LTB cell. Note the rebound bursting APs (arrow) after the termination of a hyperpolarizing current pulse in the LTB cell.

(c) Membrane responses to different current pulses recorded from the representative ES cell. ES cell has no rebound or bursting APs after the termination of a hyperpolarizing current pulse.

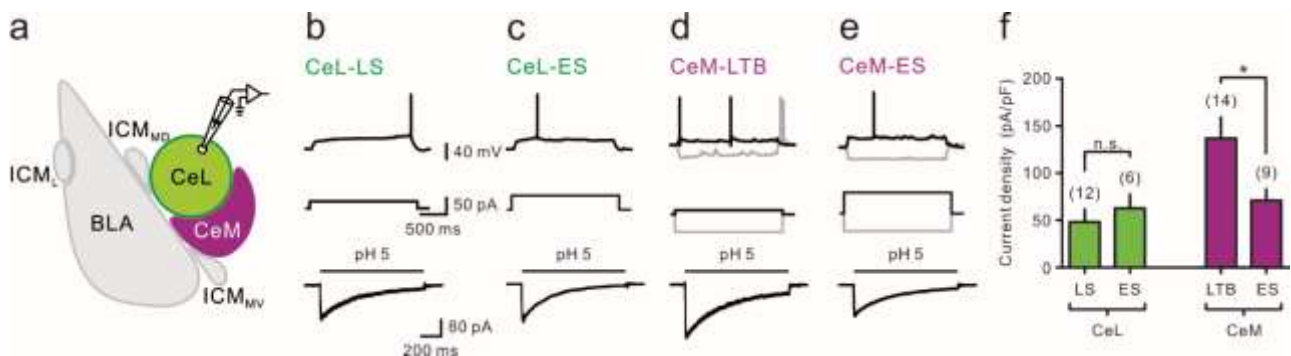


Figure 9 | Mapping of ASIC expression in major cell types of CeA

(a) Schematic diagram of whole-cell recording from CeL (green area) and CeM (purple area)

(b) – (e) Top, examples of firing patterns recorded from neurons in the CeL and CeM.

Bottom, averaged ASIC currents (CeL-LS, from 7 trials; CeL-ES, from 6 trials; CeM-LTB, from 9 trials; CeM-ES, from 14 trials) recorded from the same cell. Scale bars in

(b) apply to (c) to (e). * $P < 0.05$; n.s., not significant, Wilcoxon rank-sum test.

(f) Summary of ASIC current density. Note the high expression level of ASIC in the CeM-LTB neurons.

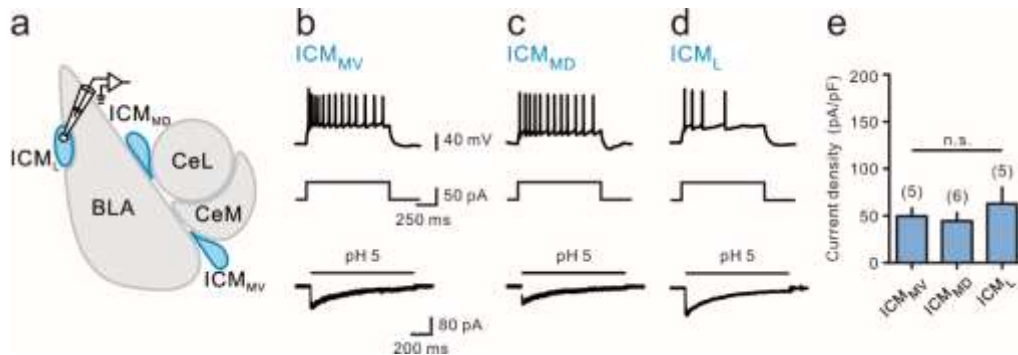


Figure 10 | Mapping of ASIC expression in ICMs

(a) Schematic diagram of whole-cell recording from ICMs (blue regions)

(b) – (d) Top, representative firing patterns of GABAergic neurons in the ICM_{MV}, ICM_{MD}, and ICM_L. Bottom, ASIC currents recorded from the same cells. Scale bars in (b) apply to (c) and (d).

(e) Summary of ASIC current density of ICM neurons. Note the modest expression level of ASICs in the ICM neurons. n.s., not significant, Wilcoxon rank-sum test.

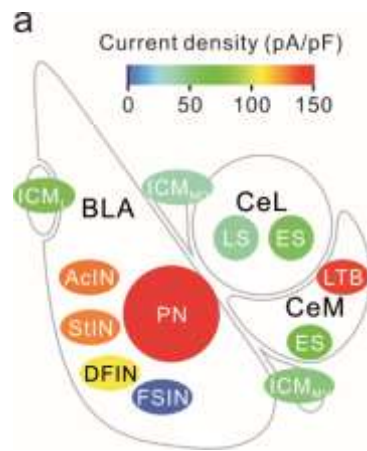


Figure 11 | Expression pattern of ASIC in the amygdala

(a) Heat map summarizing ASIC current density of various cell types of amygdala neurons. ASICs are highly expressed in the major cell types of primary input (i.e. BLA) and output (i.e. CeM) station of amygdala circuitry.

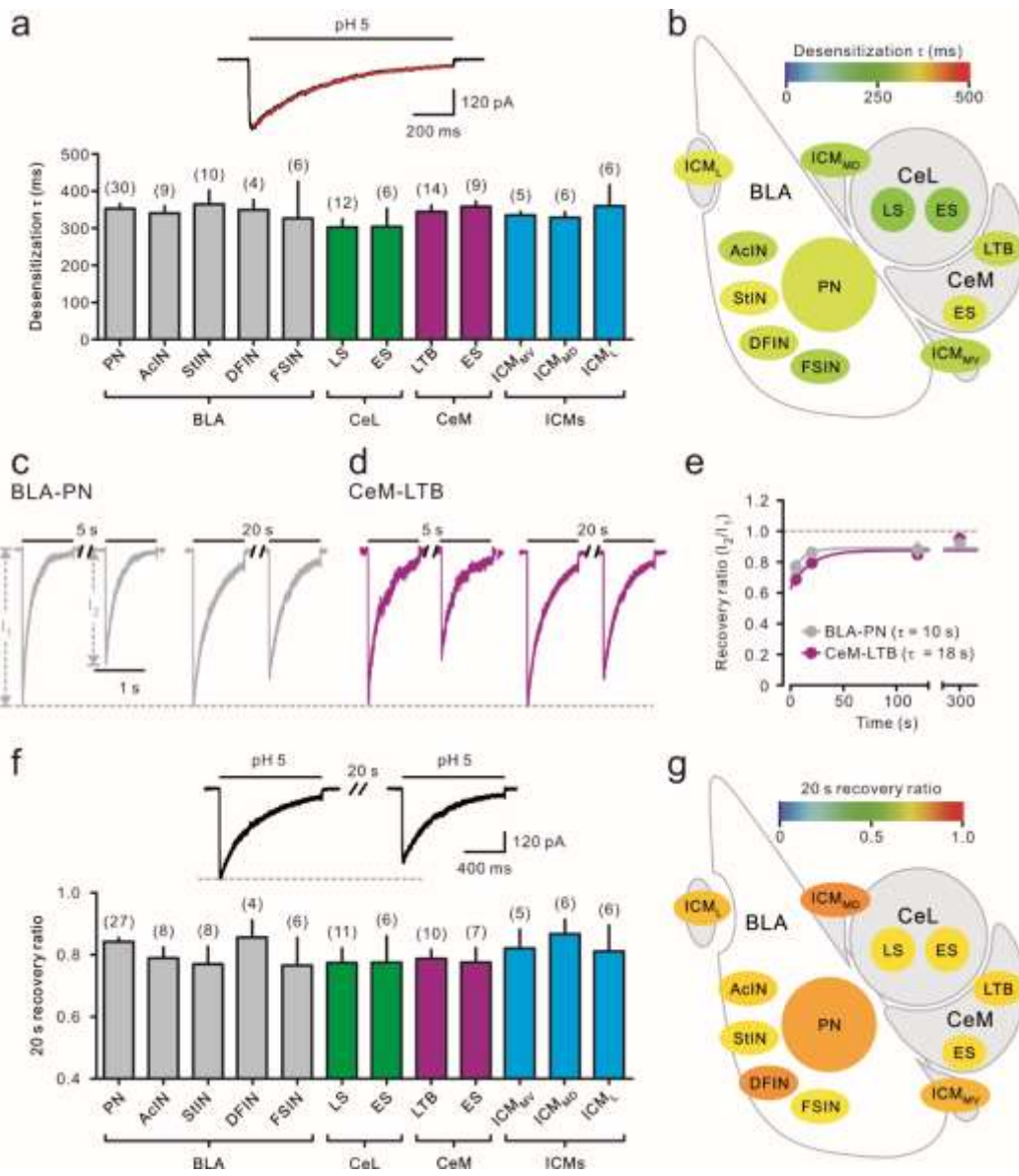


Figure 12 | ASIC current kinetics of different amygdala neurons

(a) Top, a representative ASIC current trace (black; average of 8 trials) from a BLA-PN; red curve is an exponential function fit. Bottom, bar graph showing desensitization τ of each cell type. The desensitization τ s are very similar in various types of amygdala neurons ($P = 0.52$, Kruskal-Wallis test). Numbers of patches are given in parentheses above bars.

(b) Heat map summarizing the desensitization τ s of ASIC currents of different amygdala neurons.

(c) – (d) Representative traces showing the recovery from desensitization, which were recorded from BLA-PNs (c) and CeM-LTB neurons (d), was measured at -65 mV after rapid changes from pH 7.4 to 5 for 1 s and then changed back to pH 7.4 for 5 s (left) or 20 s (right), followed by a second pulse to pH 5 for 1 s.

(e) Data points of recovery ratios (I_2/I_1) obtained from BLA-PN and CeM-LTB were fitted with a monoexponential function, yielding recovery time constants of 10 s and 18 s, respectively.

(f) Top, representative traces showing the 20 s recovery ratio was measured with 20 s inter-pulse interval. Bottom, bar graph showing the 20 s recovery ratio of ASIC currents

of each cell type. The 20 s recovery ratio of ASIC currents are very similar in various types of amygdala neurons ($P = 0.65$, Kruskal-Wallis test. Numbers of patches are given in parentheses above bars.

(g) Heat map summarizing the recovery ratios of ASIC currents of different amygdala neurons.



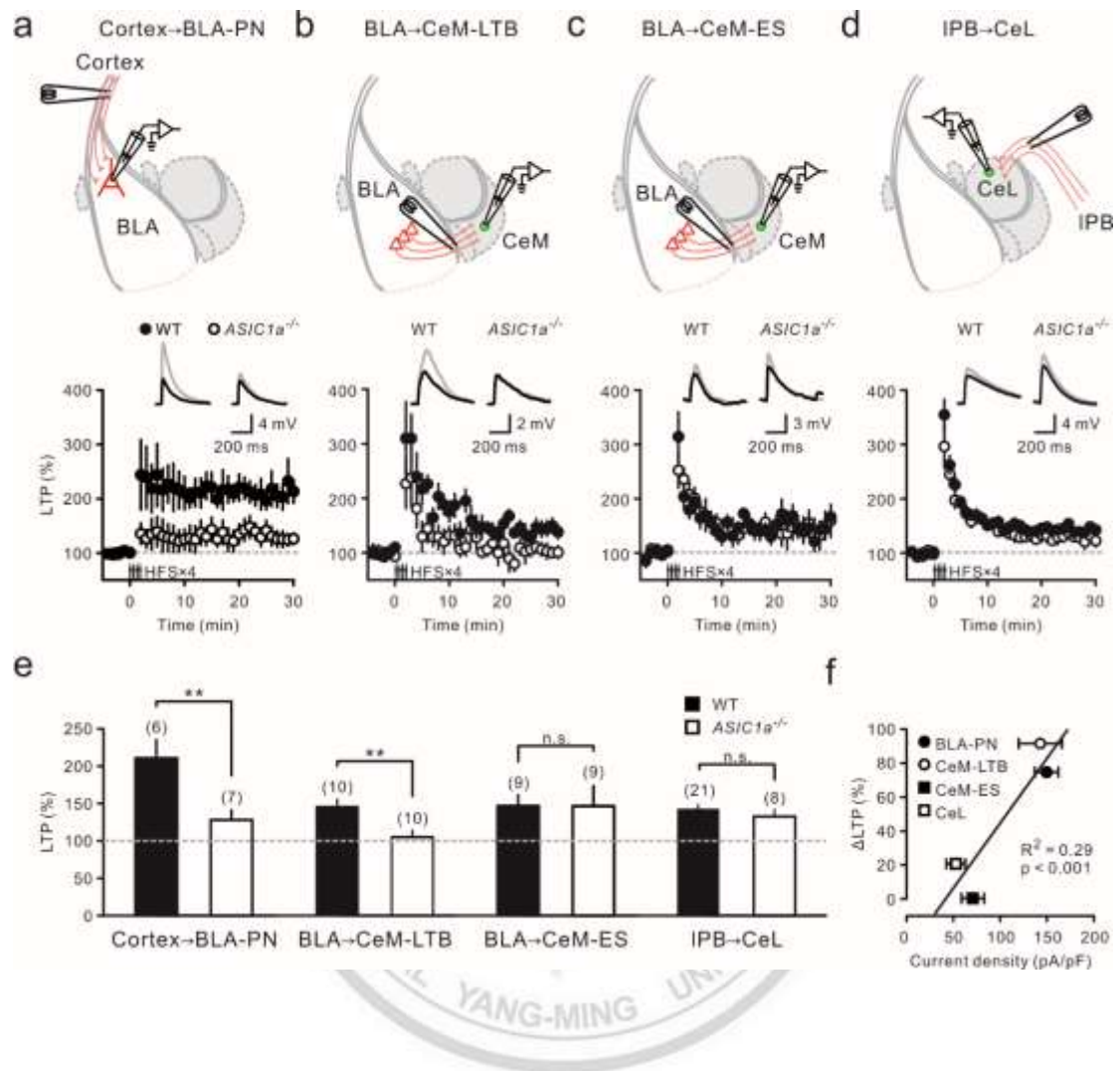


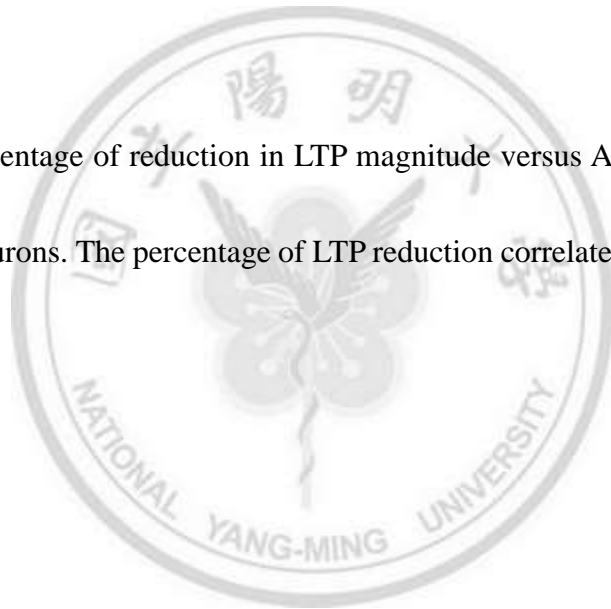
Figure 13 | ASICs selectively contributed to LTP at glutamatergic synapses onto amygdala neurons.

(a) – (d) Top, experimental configurations. Synaptic responses were measured for cortex → BLA-PN (a), BLA → CeM-LTB (b), BLA→ CeM-ES (c), and IPB → CeL (d) neuron synapses. Bottom, averaged synaptic response (normalized) plotted

against time. Representative averaged EPSP traces before (black) and after HFS (gray) were taken at the time indicated by number. (LTP at IPB → CeL neuron synapses is contributed by Ta-Chun Chien.)

(e) Summary of LTP magnitude, which was measured 25–30 min after HFS (arrow), at each synapse in WT and *ASIC1a*^{-/-} mice. **P < 0.01; n.s., not significant, Wilcoxon rank-sum test.

(f) Plot of the percentage of reduction in LTP magnitude versus ASIC current density of postsynaptic neurons. The percentage of LTP reduction correlates with ASIC current density.



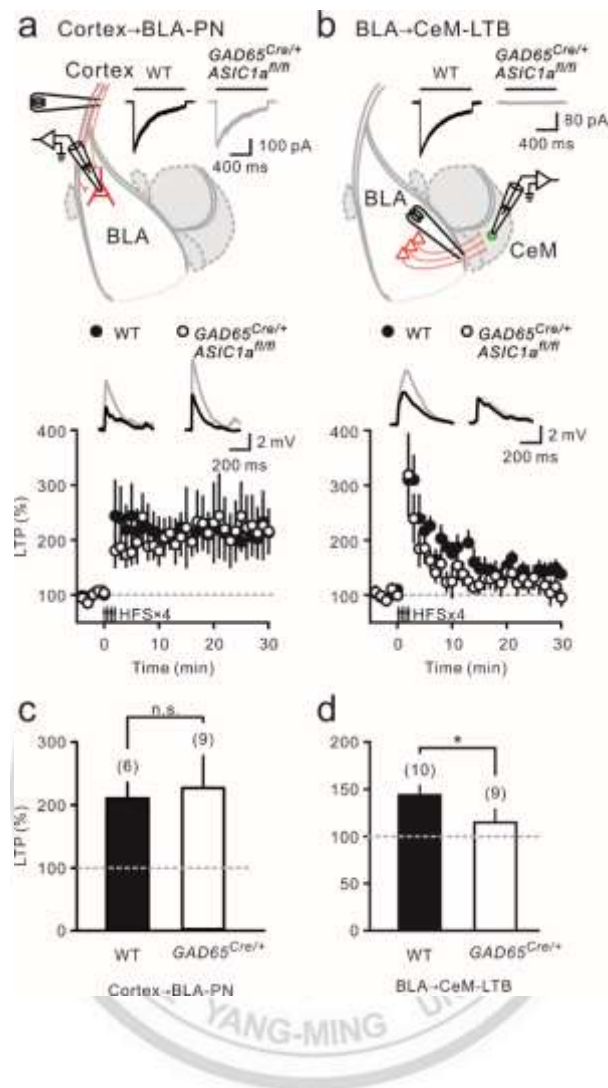
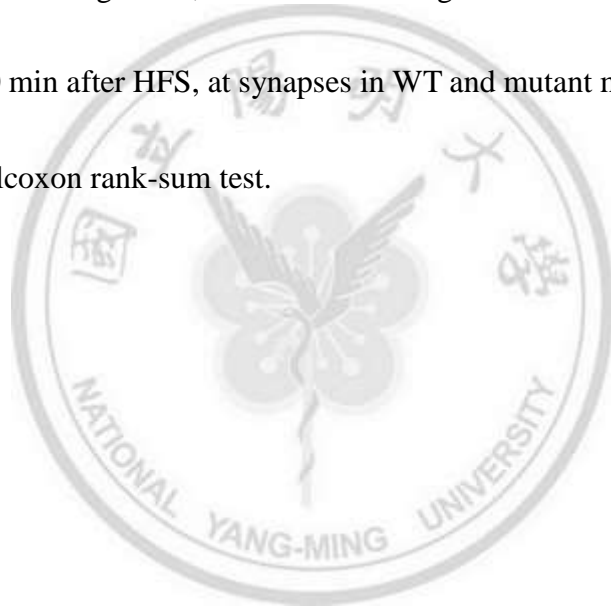


Figure 14 | ASIC1a deletion in GABAergic neurons impaired LTP at CeM-LTB neuron synapses.

(a) – (b) Top, experimental configurations. Representative ASIC current traces evoked in BLA-PN (a) and CeM-LTB neurons (b) from WT and mutant ($GAD65^{Cre/+}$;

ASIC1a^{fl/fl}) mice. Black bars denote the application of pH 5 acidic solution. Bottom, synaptic responses were measured for cortex → BLA-PN (a) and BLA → CeM-LTB neuron (b) synapses. Averaged synaptic response (normalized) plotted against time. Representative averaged EPSP traces before (black) and after HFS (gray) were taken at indicated time points.

(c–d) Summary of LTP magnitude, which is the average of the normalized postsynaptic responses at 25–30 min after HFS, at synapses in WT and mutant mice. * $P < 0.05$; n.s., not significant, Wilcoxon rank-sum test.



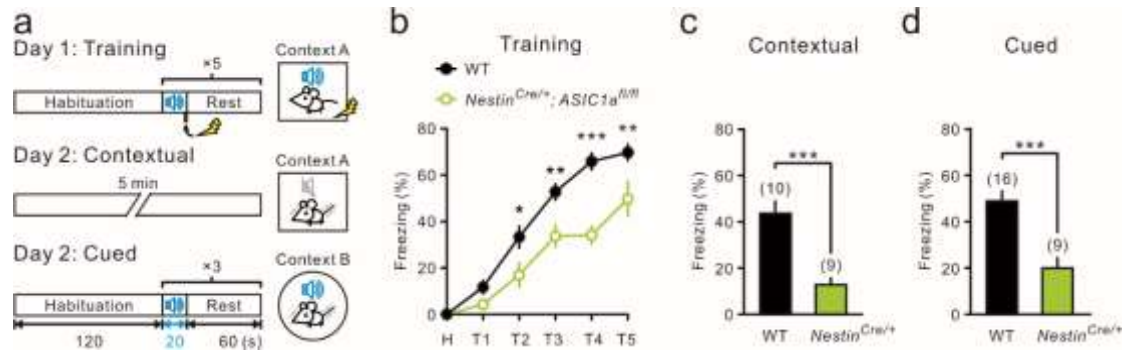


Figure 15 | Pan-neuronal deletion of ASIC1a impaired conditioned fear behavior.

(a) Experimental protocol of fear conditioning on day 1 and memory recall tests of contextual and cued fear on day 2 (see Materials and Methods).

(b) Plot of relative time spent in freezing versus the trial (T) of fear conditioning.

Nestin^{Cre/+}; ASIC1a^{fl/fl} mice have relative lower freezing level than WT mice. H, habituation. *P < 0.05; **P < 0.01; ***P < 0.001, WT versus *Nestin^{Cre/+}; ASIC1a^{fl/fl}*; ##P < 0.01; ###P < 0.001, WT vs *GAD65^{Cre/+}; ASIC1a^{fl/fl}*, Wilcoxon rank-sum test.

(c) – (d) Relative time spent in freezing during contextual and cued tests. Both contextual and cued fear are impaired in *Nestin*^{Cre/+}; *ASIC1a*^{fl/fl} mice. ****P < 0.001, Wilcoxon rank-sum test.



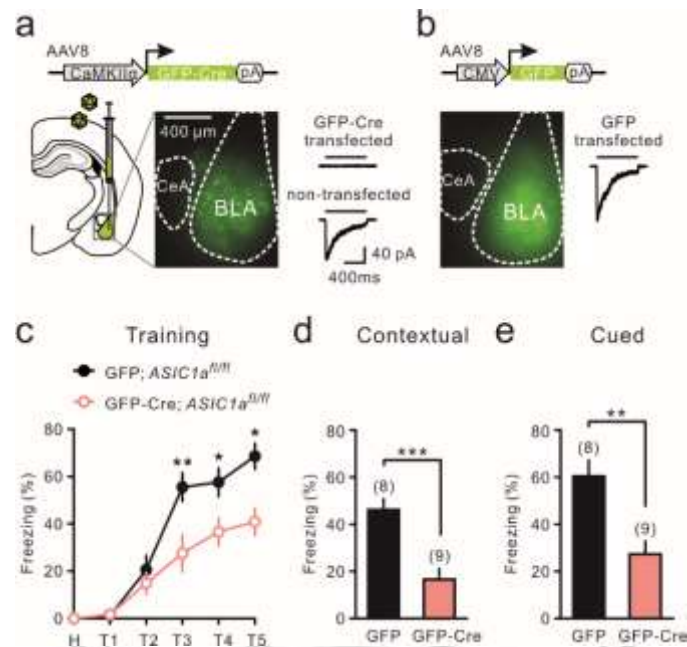


Figure 16 | Selective deletion ASIC1a in BLA-PNs impaired conditioned fear behavior.

(a) To selectively disrupt ASIC1a in BLA-PNs, AAV8 vector encoding GFP-Cre was injected into BLA of *ASIC1a^{fl/fl}* mice. Left, epifluorescence images showing GFP-Cre expression at BLA. Right, representative ASIC currents recorded from transfected and non-transfected neurons. There is no detectable ASIC current in transfected neurons. Black bars denote the application of pH 5 acidic solution. Scale bars in (a) apply to (b).

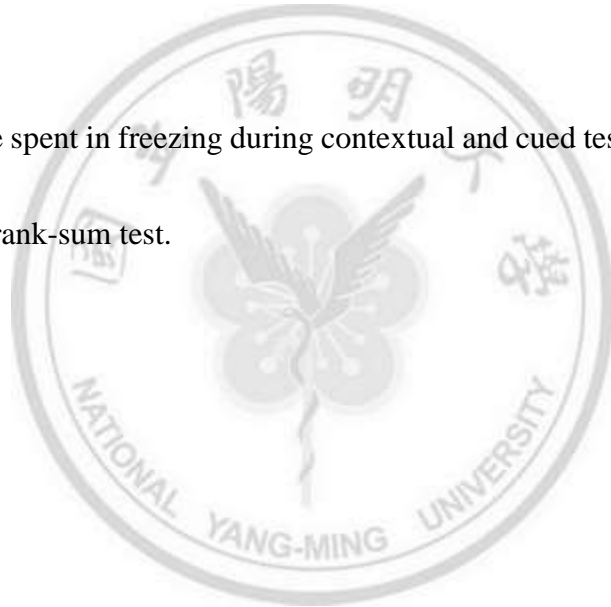
(b) AAV8 vector encoding GFP was injected into BLA of *ASIC1a^{fl/fl}* mice. Left, epifluorescence images showing GFP expression at BLA. Right, representative ASIC currents recorded from transfected neurons. Black bars denote the application of pH 5 acidic solution.

(c) Plot of relative time spent in freezing versus the trial of fear conditioning. *P < 0.05;

**P < 0.01, GFP-Cre; *ASIC1a^{fl/fl}* versus GFP; *ASIC1a^{fl/fl}*, Wilcoxon rank-sum test.

(d, e) Relative time spent in freezing during contextual and cued tests. ***P < 0.001, **P

< 0.01, Wilcoxon rank-sum test.



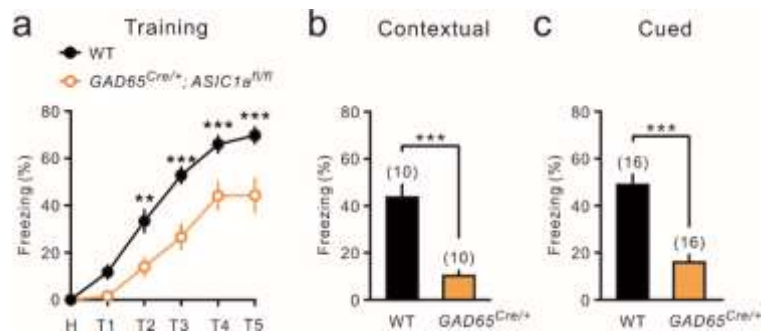


Figure 17 | Deleting ASIC1a in GABAergic neurons impaired conditioned fear behavior.

(a) Plot of relative time spent in freezing versus the trial (T) of fear conditioning. *GAD65^{Cre/+}; ASIC1a^{fl/fl}* mice have relative lower freezing level than WT mice. H, habituation. ** $P < 0.01$; *** $P < 0.001$, Wilcoxon rank-sum test.

(b) – (c) Relative time spent in freezing during contextual and cued tests. Both contextual and cued fear are impaired in *GAD65^{Cre/+}; ASIC1a^{fl/fl}* mice. *** $P < 0.001$, Wilcoxon rank-sum test. Part of behavioral experiments of *GAD65^{Cre/+}; ASIC1a^{fl/fl}* mice is contributed by Ta-Chun Chien.

Tables

Table 1 | Electrophysiological properties of neurons in the BLA

	BLA					P value
	I PN (23)	II AcIN (15)	III StIN (11)	IV DFIN (10)	V FSIN (10)	
RMP (mV)	-67.1 ± 1.3	-60.1 ± 1.5	-59.6 ± 2.7	-65.5 ± 2.0	-68.0 ± 2.4	< 0.001
	II, III, IV	I, IV, V	I, IV, V	I, II, III	II, III	
R_{in} (MΩ)	269 ± 40	330 ± 41	298 ± 57	244 ± 28	242 ± 38	0.16
Sag ratio (%)	22.9 ± 2.3	25.3 ± 4.3	24.3 ± 3.6	15.1 ± 2.3	22.8 ± 6.2	0.23
Rheobase (pA)	72.1 ± 9.7	59.5 ± 11.2	81.9 ± 24.9	91.7 ± 16.0	73.0 ± 19.2	0.45
Accommodating ratio	1.89 ± 0.01	3.44 ± 0.23	2.79 ± 0.33	1.65 ± 0.12	1.43 ± 0.06	< 0.001
	II, V	I, IV, V	IV, V	II, III	I, II, III	
Maximal CV of ISI ratios	0.42 ± 0.07	0.37 ± 0.03	1.71 ± 0.11	0.41 ± 0.10	0.13 ± 0.04	< 0.001
	III, V	III, V	I, II, IV, V	III, V	I, II, III, IV	
Spike delay (ms)	237 ± 54	121 ± 16	134 ± 23	677 ± 48	133 ± 41	< 0.001
	IV	IV	IV	IV	IV	
Maximal mean firing rate (Hz)	28.3 ± 1.3	33.8 ± 2.9	45.2 ± 6.2	38.6 ± 3.7	100.6 ± 9.6	< 0.001
	II, III, IV, V	V	V	V	V	
AP threshold (mV)	-37.1 ± 1.4	-39.3 ± 2.3	-38.4 ± 1.7	-34.0 ± 1.5	-42.3 ± 1.4	0.011
	IV	IV	IV	I, II, III, V	IV	
AP half-width (ms)	1.54 ± 0.11	0.82 ± 0.05	0.78 ± 0.05	1.18 ± 0.07	0.64 ± 0.07	< 0.001
	II, III, IV, V	I, IV	I, IV	I, II, III, V	I, IV	
AP amplitude (mV)	98.6 ± 1.3	91.7 ± 2.5	82.3 ± 2.6	74.6 ± 1.5	90.6 ± 2.9	< 0.001
	II, III, IV, V	I, III, IV	I, II, IV	I, II, III, V	I, II, IV	
AP maximum rise (V/s)	320 ± 20	311 ± 17	270 ± 18	210 ± 16	327 ± 22	0.001
	IV	IV	IV	I, II, III, V	IV	
AP maximum decay (V/s)	-57 ± 15	-105 ± 13	-111 ± 10	-59 ± 11	-184 ± 8	< 0.001
	II, III, V	I, IV, V	I, IV, V	II, III, V	I, II, III, IV	

Numbers of cells are given in parentheses. Kruskal-Wallis test was performed to compare the means among groups. All values are given as mean ± s.e.m. Statistical

differences between PNs and four types of INs, estimated based on Wilcoxon rank-sum test after Kruskal-Wallis test, are marked under the corresponding parameter, $P < 0.05$.

RMP, resting membrane potential; R_{in} , input resistance.



Table 2 | Electrophysiological properties of the major cell types in the CeL

	CeL		P value
	LS (46)	ES (26)	
RMP (mV)	-70.8 ± 1.4	-65.7 ± 2.2	0.033
R_{in} (MΩ)	420 ± 25	415 ± 36	0.038
Sag ratio (%)	17.6 ± 2.3	24.3 ± 3.1	0.017
Rheobase (pA)	37.6 ± 2.7	31.8 ± 3.0	0.17
Spike delay (ms)	1769 ± 24	778 ± 86	< 0.001
Ramp ratio	1.37 ± 0.02	0.93 ± 0.02	< 0.001
AP threshold (mV)	-34.8 ± 0.7	-33.1 ± 1.1	0.30
AP half-width (ms)	2.03 ± 0.11	1.63 ± 0.13	< 0.001
AP amplitude (mV)	89.3 ± 1.1	90.5 ± 2.3	0.11
AP maximum rise (V/s)	218 ± 9	241 ± 14	0.06
AP maximum decay (V/s)	-42 ± 44	-54 ± 25	0.008

Wilcoxon rank-sum test was performed to determine statistical significance between the groups. Numbers of cells are given in parentheses. All values are given as mean ± s.e.m.

Table 3 | Electrophysiological properties of the major cell types in the CeM

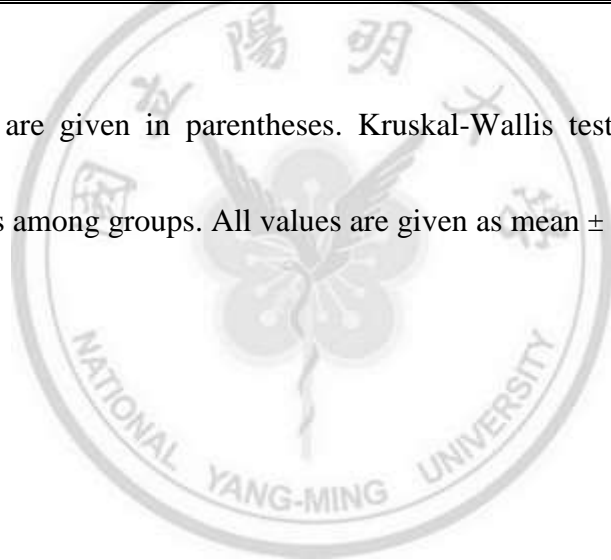
	CeM		P value
	LTB (37)	ES (29)	
RMP (mV)	-58.0 ± 1.2	-61.7 ± 2.0	0.07
R_{in} (MΩ)	568 ± 42	589 ± 50	0.71
Sag ratio (%)	43.7 ± 4.0	18.0 ± 1.8	< 0.001
Rheobase (pA)	21.1 ± 1.8	33.2 ± 4.0	0.013
AP threshold (mV)	-39.5 ± 0.9	-35.8 ± 1.2	0.007
AP half-width (ms)	1.17 ± 0.03	1.33 ± 0.07	0.06
AP amplitude (mV)	92.5 ± 1.2	91.1 ± 1.6	0.52
AP maximum rise (V/s)	254 ± 9	248 ± 10	0.59
AP maximum decay (V/s)	-74 ± 38	-66 ± 29	0.05

Wilcoxon rank-sum test was performed to determine the statistical significance between the groups. Numbers of cells are given in parentheses. All values are given as mean ± s.e.m.

Table 4 | Electrophysiological properties of neurons in the ICMs

	ICM_{MV} (16)	ICM_{MD} (12)	ICM_L (8)	P value
RMP (mV)	-65.3 ± 2.2	-66.3 ± 1.3	-71.1 ± 2.5	0.10
R_{in} (MΩ)	693 ± 77	709 ± 60	692 ± 72	0.73
Sag ratio (%)	18.1 ± 2.3	18.5 ± 4.6	21.6 ± 5.0	0.54
Rheobase (pA)	32.6 ± 3.4	34.9 ± 5.9	37.3 ± 3.3	0.42
AP threshold (mV)	-32.9 ± 1.4	-33.5 ± 1.2	-31.8 ± 2.6	0.90
AP half-width (ms)	1.14 ± 0.06	1.08 ± 0.04	1.21 ± 0.05	0.25
AP amplitude (mV)	86.9 ± 1.9	88.4 ± 1.9	85.6 ± 2.7	0.48
AP maximum rise (V/s)	228 ± 12	227 ± 10	200 ± 15	0.28
AP maximum decay (V/s)	-72 ± 16	-76 ± 13	-66 ± 9	0.10

Numbers of cells are given in parentheses. Kruskal-Wallis test was performed to compare the means among groups. All values are given as mean ± s.e.m.



References

Alvarez de la Rosa D, Krueger SR, Kolar A, Shao D, Fitzsimonds RM, Canessa CM. (2003) Distribution, subcellular localization and ontogeny of ASIC1 in the mammalian central nervous system. *J Physiol* **546**, 77-87.

Amano T, Unal CT, Paré D. (2010) Synaptic correlates of fear extinction in the amygdala. *Nat Neurosci* **13**, 489-494.

Amano T, Duvarci S, Popa D, Paré D. (2011) The fear circuit revisited: contributions of the basal amygdala nuclei to conditioned fear. *J Neurosci* **31**, 15481-15489.

Askwith CC, Wemmie JA, Price MP, Rokhlina T, Welsh MJ. (2004) Acid-sensing ion channel 2. (ASIC2) modulates ASIC1 H⁺-activated currents in hippocampal neurons. *J Biol Chem* **279**, 18296-18305.

Baron A, Waldmann R, Lazdunski M. (2002) ASIC-like, proton-activated currents in rat hippocampal neurons. *J Physiol* **539**, 485-494.

Baron A, Voilley N, Lazdunski M, Lingueglia E. (2008) Acid sensing ion channels in dorsal spinal cord neurons. *J Neurosci* **28**, 1498-1508.

Bartoi T, Augustinowski K, Polleichtner G, Gründer S, Ulbrich MH. (2014) Acid-sensing ion channel (ASIC) 1a/2a heteromers have a flexible 2:1/1:2 stoichiometry. *Proc Natl Acad Sci U S A* **111**, 8281-8286.

Battaglia M, Perna G. (1995) The 35% CO₂ challenge in panic disorder: optimization by receiver operating characteristic (ROC) analysis. *J Psychiatr Res* **29**, 111-119.

Battaglia M, Ogliari A. (2005) Anxiety and panic: from human studies to animal research and back. *Neurosci Biobehav Rev* **29**, 169-179.

Biagini G, Babinski K, Avoli M, Marcinkiewicz M, Séguéla P. (2001) Regional and subunit-specific downregulation of acid-sensing ion channels in the pilocarpine model of epilepsy. *Neurobiol Dis* **8**, 45-58.

Boiko N, Kucher V, Wang B, Stockand JD. (2014) Restrictive expression of acid-sensing ion channel 5. (Asic5) in unipolar brush cells of the vestibulocerebellum. *PLoS One* **9**, e91326.

Bolshakov KV, Essin KV, Buldakova SL, Dorofeeva NA, Skatchkov SN, Eaton MJ, Tikhonov DB, Magazanik LG. (2002) Characterization of acid-sensitive ion channels in freshly isolated rat brain neurons. *Neuroscience* **110**, 723-730.

Cauli B, Porter JT, Tsuzuki K, Lambolez B, Rossier J, Quenet B, Audinat E. (2000) Classification of fusiform neocortical interneurons based on unsupervised clustering. *Proc Natl Acad Sci U S A* **97**, 6144-6149.

Chan CF, Kuo TW, Weng JY, Lin YC, Chen TY, Cheng JK, Lien CC. (2013) Ba²⁺- and bupivacaine-sensitive background K⁺ conductances mediate rapid EPSP attenuation in oligodendrocyte precursor cells. *J Physiol* **591**, 4843-4858.

Chen X, Kalbacher H, Gründer S. (2005) The tarantula toxin psalmotoxin 1 inhibits acid-sensing ion channel. (ASIC) 1a by increasing its apparent H⁺ affinity. *J Gen Physiol* **126**, 71-79.

Chesler M, Kaila K. (1993) Modulation of pH by neuronal activity. *Trends Neurosci* **15**, 396-402.

Cho JH, Askwith CC. (2008) Presynaptic release probability is increased in hippocampal neurons from ASIC1 knockout mice. *J Neurophysiol* **99**, 426-441.

Ciocchi S, Herry C, Grenier F, Wolff SB, Letzkus JJ, Vlachos I, Ehrlich I, Sprengel R, Deisseroth K, Stadler MB, Müller C, Lüthi A. (2010) Encoding of conditioned fear in central amygdala inhibitory circuits. *Nature* **468**, 277-282.

Coryell MW, Ziemann AE, Westmoreland PJ, Haenfler JM, Kurjakovic Z, Zha XM, Price M, Schnizler MK, Wemmie JA. (2007) Targeting ASIC1a reduces innate fear and alters neuronal activity in the fear circuit. *Biol Psychiatry* **62**, 1140-1148.

Coryell MW, Wunsch AM, Haenfler JM, Allen JE, McBride JL, Davidson BL, Wemmie JA. (2008) Restoring acid-sensing ion channel-1a in the amygdala of knock-out mice rescues fear memory but not unconditioned fear responses. *J Neurosci* **28**, 13738-13741.

Coryell MW, Wunsch AM, Haenfler JM, Allen JE, Schnizler M, Ziemann AE, Cook MN, Dunning JP, Price MP, Rainier JD, Liu Z, Light AR, Langbehn DR, Wemmie JA. (2009) Acid-sensing ion channel-1a in the amygdala, a novel therapeutic target in depression-related behavior. *J Neurosci* **29**, 5381-5388.

Deval E, Lingueglia E. (2015) Acid-Sensing Ion Channels and nociception in the peripheral and central nervous systems. *Neuropharmacology* doi: 10.1016/j.neuropharm.2015.02.009. [Epub ahead of print]

Diochot S, Baron A, Rash LD, Deval E, Escoubas P, Scarzello S, Salinas M, Lazdunski M. (2004) A new sea anemone peptide, APETx2, inhibits ASIC3, a major acid-sensitive channel in sensory neurons. *EMBO J* **23**, 1516-1525.

Diochot S, Baron A, Salinas M, Douguet D, Scarzello S, Dabert-Gay AS, Debayle D, Friend V, Alloui A, Lazdunski M, Lingueglia E. (2012) Black mamba venom peptides target acid-sensing ion channels to abolish pain. *Nature* **25**, 552-555

Du J, Reznikov LR, Price MP, Zha XM, Lu Y, Moninger TO, Wemmie JA, Welsh MJ. (2014) Protons are a neurotransmitter that regulates synaptic plasticity in the lateral amygdala. *Proc Natl Acad Sci U S A* **111**, 8961-8966.

Duvarci S, Popa D, Paré D. (2011) Central amygdala activity during fear conditioning. *J Neurosci* **31**, 289-294.

Duvarci S, Paré D. (2014) Amygdala microcircuits controlling learned fear. *Neuron* **82**, 966-980.

Ehrlich I, Humeau Y, Grenier F, Cioocchi S, Herry C, Lüthi A. (2009) Amygdala inhibitory circuits and the control of fear memory. *Neuron* **62**, 757-771.

Fourcaudot E, Gambino F, Casassus G, Poulain B, Humeau Y, Lüthi A. (2009) L-type voltage-dependent Ca²⁺ channels mediate expression of presynaptic LTP in amygdala. *Nat Neurosci* **12**, 1093-1095.

Fu Y, Pollandt S, Liu J, Krishnan B, Genzer K, Orozco-Cabal L, Gallagher JP, Shinnick-Gallagher P. (2007) Long-term potentiation. (LTP) in the central amygdala. (CeA) is enhanced after prolonged withdrawal from chronic cocaine and requires CRF₁ receptors. *J Neurophysiol* **97**, 937-941.

Gao J, Duan B, Wang DG, Deng XH, Zhang GY, Xu L, Xu TL. (2005) Coupling between NMDA receptor and acid-sensing ion channel contributes to ischemic neuronal death. *Neuron* **48**, 635-646.

Gentet LJ, Stuart GJ, Clements JD. (2000) Direct measurement of specific membrane capacitance in neurons. *Biophys J* **79**, 314-320.

Goosens KA, Maren S. (2001) Contextual and auditory fear conditioning are mediated by the lateral, basal, and central amygdaloid nuclei in rats. *Learn Mem* **8**, 148-155.

Goosens KA, Maren S. (2003) Pretraining NMDA receptor blockade in the basolateral complex, but not the central nucleus, of the amygdala prevents savings of conditional fear. *Behav Neurosci* **117**, 738-750.

Graebenitz S, Kedo O, Speckmann EJ, Gorji A, Panneck H, Hans V, Palomero-Gallagher N, Schleicher A, Zilles K, Pape HC. (2011) Interictal-like network activity and receptor expression in the epileptic human lateral amygdala. *Brain* **134**, 2929-2947.

Haubensak W, Kunwar PS, Cai H, Ciocchi S, Wall NR, Ponnusamy R, Biag J, Dong HW, Deisseroth K, Callaway EM, Fanselow MS, Lüthi A, Anderson DJ. (2010) Genetic dissection of an amygdala microcircuit that gates conditioned fear. *Nature* **468**, 270-276.

Herry C, Ciocchi S, Senn V, Demmou L, Müller C, Lüthi A. (2008) Switching on and off fear by distinct neuronal circuits. *Nature* **454**, 600-606.

Hille B. (2001) *Ion channels of excitable membranes*. 3rd ed, Sunderland, MA: Sinauer Associates.

Immke DC, McCleskey EW. (2003) Protons open acid-sensing ion channels by catalyzing relief of Ca²⁺ blockade. *Neuron* **37**, 75-84.

Jasnow AM, Ressler KJ, Hammack SE, Chhatwal JP, Rainnie DG. (2009) Distinct subtypes of cholecystokinin (CCK)-containing interneurons of the basolateral amygdala identified using a CCK promoter-specific lentivirus. *J Neurophysiol* **101**, 1494-1506.

Jasti J, Furukawa H, Gonzales EB, Gouaux E. (2007) Structure of acid-sensing ion channel 1 at 1.9 Å resolution and low pH. *Nature* **449**, 316-323.

Jüngling K, Seidenbecher T, Sosulina L, Lesting J, Sangha S, Clark SD, Okamura N, Duangdao DM, Xu YL, Reinscheid RK, Pape HC. (2008) Neuropeptide S-mediated control of fear expression and extinction: role of intercalated GABAergic neurons in the amygdala. *Neuron* **59**, 298-310.

Katona I, Rancz EA, Acsady L, Ledent C, Mackie K, Hajos N, Freund TF. (2001) Distribution of CB1 cannabinoid receptors in the amygdala and their role in the control of GABAergic transmission. *J Neurosci* **21**, 9506-9518.

Kellenberger S, Schild L. (2002) Epithelial sodium channel/degenerin family of ion channels: a variety of functions for a shared structure. *Physiol Rev* **82**, 735-767.

Kreple CJ, Lu Y, Taugher RJ, Schwager-Gutman AL, Du J, Stump M, Wang Y, Ghobbeh A, Fan R, Cosme CV, Sowers LP, Welsh MJ, Radley JJ, LaLumiere RT, Wemmie JA. (2014) Acid-sensing ion channels contribute to synaptic transmission and inhibit cocaine-evoked plasticity. *Nat Neurosci* **17**, 1083-1091.

Krishtal OA, Pidoplichko VI. (1980) A receptor for protons in the nerve cell membrane. *Neuroscience* **5**, 2325-2327.

LeDoux JE. (2000) Emotion circuits in the brain. *Annu Rev Neurosci* **23**, 155-184.

Lévesque M, Avoli M. (2013) The kainic acid model of temporal lobe epilepsy. *Neurosci Biobehav Rev* **37**, 2887-2899.

Li H, Penzo MA, Taniguchi H, Kopec CD, Huang ZJ, Li B. (2013) Experience-dependent modification of a central amygdala fear circuit. *Nat Neurosci* **16**, 332-339.

Lien CC, Jonas P. (2003) Kv3 potassium conductance is necessary and kinetically optimized for high-frequency action potential generation in hippocampal interneurons. *J Neurosci* **23**, 2058-2068.

Lien CC, Martina M, Schultz JH, Ehmke H, Jonas P. (2002) Gating, modulation and subunit composition of voltage-gated K⁺ channels in dendritic inhibitory interneurons of rat hippocampus. *J Physiol* **538**, 405-419.

Likhtik E, Popa D, Apergis-Schoute J, Fidacaro GA, Paré D. (2008) Amygdala intercalated neurons are required for expression of fear extinction. *Nature* **454**, 642-645.

Lin YC, Liu YC, Huang YY, Lien CC. (2010) High-density expression of Ca²⁺-permeable ASIC1a channels in NG2 glia of rat hippocampus. *PloS One* **5**, e12665.

Lingueglia E. (2007) Acid-sensing ion channels in sensory perception. *J Biol Chem* **282**, 17325-17329.

López de Armentia M, Sah P. (2007) Bidirectional synaptic plasticity at nociceptive afferents in the rat central amygdala. *J Physiol* **581**, 961-970.

Maren S. (2008) Pavlovian fear conditioning as a behavioral assay for hippocampus and amygdala function: cautions and caveats. *Eur J Neurosci* **28**, 1661-1666

Mascagni F, McDonald AJ. (2003) Immunohistochemical characterization of cholecystinin containing neurons in the rat basolateral amygdala. *Brain Res* **976**, 171-184.

McDonald AJ. (1982) Cytoarchitecture of the central amygdaloid nucleus of the rat. *J Comp Neurol* **208**, 401-418.

McKernan MG, Shinnick-Gallagher P. (1997) Fear conditioning induces a lasting potentiation of synaptic currents in vitro. *Nature* **390**, 607-611.

Myers KM, Davis M. (2007) Mechanisms of fear extinction. *Mol Psychiatry* **12**, 120-150.

Paré D, Royer S, Smith Y, Lang EJ. (2003) Contextual inhibitory gating of impulse traffic in the intra-amygdaloid network. *Ann N Y Acad Sci* **985**, 78-91.

Paré D, Duvarci S. (2012) Amygdala microcircuits mediating fear expression and extinction. *Curr Opin Neurobiol* **22**, 717-723.

Pi HJ, Hangya B, Kvitsiani D, Sanders JI, Huang ZJ, Kepecs A. (2013) Cortical interneurons that specialize in disinhibitory control. *Nature* **503**, 521-524.

Pidoplichko VI, Aroniadou-Anderjaska V, Prager EM, Figueiredo TH, Almeida-Suhett CP, Miller SL, Braga MF. (2014) ASIC1a activation enhances inhibition in the basolateral amygdala and reduces anxiety. *J Neurosci* **34**, 3130-3141.

Popescu AT, Paré D. (2011) Synaptic interactions underlying synchronized inhibition in the basal amygdala: evidence for existence of two types of projection cells. *J Neurophysiol* **105**, 687-696.

Price MP, Lewin GR, McIlwrath SL, Cheng C, Xie J, Heppenstall PA, Stucky CL, Mannsfeldt AG, Brennan TJ, Drummond HA, Qiao J, Benson CJ, Tarr DE, Hrstka RF, Yang B, Williamson RA, Welsh MJ. (2000) The mammalian sodium channel BNC1 is required for normal touch sensation. *Nature* **407**, 1007-1011.

Price MP, Gong H, Parsons MG, Kundert JR, Reznikov LR, Bernardinelli L, Chaloner K, Buchanan GF, Wemmie JA, Richerson GB, Cassell MD, Welsh MJ. (2014)

Localization and behaviors in null mice suggest that ASIC1 and ASIC2 modulate responses to aversive stimuli. *Genes Brain Behav* **13**, 179-194.

Rogan MT, Stäubli UV, LeDoux JE. (1997) Fear conditioning induces associative long-term potentiation in the amygdala. *Nature* **390**, 604-607.

Sah P, Faber ES, Lopez De Armentia M, Power J. (2003) The amygdaloid complex: anatomy and physiology. *Physiol Rev* **83**, 803-834.

Sah P, Westbrook RF, Lüthi A. (2008) Fear conditioning and long-term potentiation in the amygdala: what really is the connection? *Ann N Y Acad Sci* **1129**, 88-95.

Sakai H, Lingueglia E, Champigny G, Mattei MG, Lazdunski M. (1999) Cloning and functional expression of a novel degenerin-like Na⁺ channel gene in mammals. *J Physiol* **519**, 323-333.

Schramm J. (2008) Temporal lobe epilepsy surgery and the quest for optimal extent of resection: a review. *Epilepsia* **49**, 1296-1307.

Sherwood TW, Lee KG, Gormley MG, Askwith CC. (2011) Heteromeric acid-sensing ion channels. (ASICs) composed of ASIC2b and ASIC1a display novel channel properties and contribute to acidosis-induced neuronal death. *J Neurosci* **31**, 9723-9734.

Shin RM, Tsvetkov E, Bolshakov VY. (2006) Spatiotemporal asymmetry of associative synaptic plasticity in fear conditioning pathways. *Neuron* **52**, 883-896.

Smoller JW, Gallagher PJ, Duncan LE, McGrath LM, Haddad SA, Holmes AJ, Wolf AB, Hilker S, Block SR, Weill S, Young S, Choi EY, Rosenbaum JF, Biederman J, Faraone SV, Roffman JL, Manfro GG, Blaya C, Hirshfeld-Becker DR, Stein MB, Van Ameringen M, Tolin DF, Otto MW, Pollack MH, Simon NM, Buckner RL, Ongür D,

Cohen BM. (2014) The Human Ortholog of Acid-Sensing Ion Channel Gene ASIC1a Is Associated with Panic Disorder and Amygdala Structure and Function. *Biol Psychiatry* **76**, 902-910

Song C, Xu XB, He Y, Liu ZP, Wang M, Zhang X, Li BM, Pan BX. (2013) Stuttering interneurons generate fast and robust inhibition onto projection neurons with low capacity of short term modulation in mouse lateral amygdala. *PLoS One* **8**, e60154.

Sosulina L, Graebenitz S, Pape HC. (2010) GABAergic interneurons in the mouse lateral amygdala: a classification study. *J Neurophysiol* **104**, 617-626.

Spampanato J, Polepalli J, Sah P. (2011) Interneurons in the basolateral amygdala. *Neuropharmacology* **60**, 765-773

Stadler H, Tsukita S. (1984) Synaptic vesicles contain an ATP-dependent proton pump and show 'knob-like' protrusions on their surface. *EMBO J* **3**, 3333-3337.

Tamamaki N, Yanagawa Y, Tomioka R, Miyazaki J, Obata K, Kaneko T. (2003) Green fluorescent protein expression and colocalization with calretinin, parvalbumin, and somatostatin in the GAD67-GFP knock-in mouse. *J Comp Neurol* **467**, 60-79.

Trouche S, Sasaki JM, Tu T, Reijmers LG. (2013) Fear extinction causes target-specific remodeling of perisomatic inhibitory synapses. *Neuron* **80**, 1054-1065.

Ugawa S, Ueda T, Takahashi E, Hirabayashi Y, Yoneda T, Komai S, Shimada S. (2001) Cloning and functional expression of ASIC- β 2, a splice variant of ASIC- β . *Neuroreport* **12**, 2865-2869.

Viviani D, Charlet A, van den Burg E, Robinet C, Hurni N, Abatis M, Magara F, Stoop R. (2011) Oxytocin selectively gates fear responses through distinct outputs from the central amygdala. *Science* **333**, 104-107.

Waldmann R, Champigny G, Bassilana F, Heurteaux C, Lazdunski M. (1997) A proton-gated cation channel involved in acid-sensing. *Nature* **386**, 173-177.

Ward JH Jr. (1963) Hierarchical grouping to optimize an objective function. *J Am Stat Assoc* **58**, 236-244.

Watabe AM, Ochiai T, Nagase M, Takahashi Y, Sato M, Kato F. (2013) Synaptic potentiation in the nociceptive amygdala following fear learning in mice. *Mol Brain* **6**, 11.

Wemmie JA, Chen J, Askwith CC, Hruska-Hageman AM, Price MP, Nolan BC, Yoder PG, Lamani E, Hoshi T, Freeman JH Jr, Welsh MJ. (2002) The acid-activated ion channel ASIC contributes to synaptic plasticity, learning, and memory. *Neuron* **34**, 463-477.

Wemmie JA, Askwith CC, Lamani E, Cassell MD, Freeman JH Jr, Welsh MJ. (2003) Acid-sensing ion channel 1 is localized in brain regions with high synaptic density and contributes to fear conditioning. *J Neurosci* **23**, 5496-5502.

Wemmie JA, Coryell MW, Askwith CC, Lamani E, Leonard AS, Sigmund CD, Welsh MJ. (2004) Overexpression of acid-sensing ion channel 1a in transgenic mice increases acquired fear-related behavior. *Proc Natl Acad Sci U S A* **101**, 3621-3626.

Wemmie JA, Price MP, Welsh MJ. (2006) Acid-sensing ion channels: advances, questions and therapeutic opportunities. *Trends Neurosci* **29**, 578-586.

Wemmie JA, Taugher RJ, Kreple CJ. (2013) Acid-sensing ion channels in pain and disease. *Nat Rev Neurosci* **14**, 461-471.

Weng JY, Lin YC, Lien CC. (2010) Cell type-specific expression of acid-sensing ion channels in hippocampal interneurons. *J Neurosci* **30**, 6548-6558.

Wessa P. (2014) Free Statistics Software, Office for Research Development and Education, version 1.1.23-r7, URL <http://www.wessa.net/>

Wiemuth D, Gründer S. (2010) A single amino acid tunes Ca²⁺ inhibition of brain liver intestine Na⁺ channel (BLINaC). *J Biol Chem* **285**, 30404-30410.

Wolff SB, Gründemann J, Tovote P, Krabbe S, Jacobson GA, Müller C, Herry C, Ehrlich I, Friedrich RW, Letzkus JJ, Lüthi A. (2014) Amygdala interneuron subtypes control fear learning through disinhibition. *Nature* **509**, 453-458.

Woodruff AR, Sah P. (2007) Networks of parvalbumin-positive interneurons in the basolateral amygdala. *J Neurosci* **27**, 553-563.

Wu PY, Huang YY, Chen CC, Hsu TT, Lin YC, Weng JY, Chien TC, Cheng IH, Lien CC. (2013) Acid-sensing ion channel-1a is not required for normal hippocampal LTP and spatial memory. *J Neurosci* **33**, 1828-1832.

Yermolaieva O, Leonard AS, Schnizler MK, Abboud FM, Welsh MJ. (2004) Extracellular acidosis increases neuronal cell calcium by activating acid-sensing ion channel 1a. *Proc Natl Acad Sci U S A* **101**, 6752-6757.

Xiong ZG, Pignataro G, Li M, Chang SY, Simon RP. (2008) Acid-sensing ion channels. (ASICs) as pharmacological targets for neurodegenerative diseases. *Curr Opin Pharmacol* **8**, 25-32.

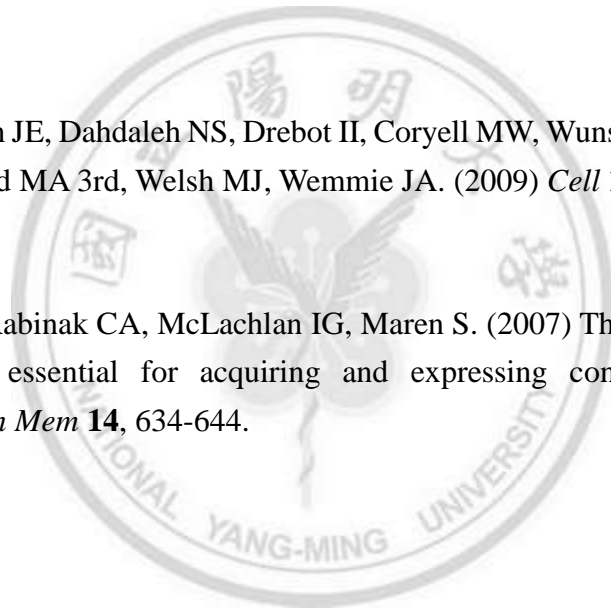
Zha XM, Wemmie JA, Green SH, Welsh MJ. (2006) Acid-sensing ion channel 1a is a postsynaptic proton receptor that affects the density of dendritic spines. *Proc Natl Acad Sci U S A* **103**, 16556-16561.

Zha XM, Costa V, Harding AM, Reznikov L, Benson CJ, Welsh MJ. (2009) ASIC2 subunits target acid-sensing ion channels to the synapse via an association with PSD-95. *J Neurosci* **29**, 8438-8446.

Ziemann AE, Schnizler MK, Albert GW, Severson MA, Howard MA 3rd, Welsh MJ, Wemmie JA. (2008) Seizure termination by acidosis depends on ASIC1a. *Nat Neurosci* **11**, 816-822.

Ziemann AE, Allen JE, Dahdaleh NS, Drebot II, Coryell MW, Wunsch AM, Lynch CM, Faraci FM, Howard MA 3rd, Welsh MJ, Wemmie JA. (2009) *Cell* **139**, 1012-10121.

Zimmerman JM, Rabinak CA, McLachlan IG, Maren S. (2007) The central nucleus of the amygdala is essential for acquiring and expressing conditional fear after overtraining. *Learn Mem* **14**, 634-644.



Curriculum Vitae

江柏翰 Chiang, Po-Han

Phone: +886-912-060-525

e-mail: Chiang@live.com

Address: 16F-1, No.219, Jixian Rd., Luzhou Dist., New Taipei City 247, Taiwan (R.O.C.)

EDUCATION

2009~2015 **Ph.D. in Neuroscience**. Institute of Neuroscience, National Yang-Ming University, Taipei, Taiwan

2005~2009 **B.S. in Life Science**. Faculty of Life Science, National Yang-Ming University, Taipei, Taiwan

RESEARCH INTERESTS

Neuronal Circuitry of Emotion, Network Modeling, Functional Connectome, Brain-Machine Interface.

PUBLICATION

1. **Chiang PH**, Chien TC, Chen CC, Yanagawa Y, Lien CC. (2015) ASIC-dependent LTP at multiple glutamatergic synapses in amygdala network is required for fear memory. *Scientific Reports* 5:10143 (Impact Factor: 5.6; Rank: Top 9.1% in Category of Multidisciplinary Sciences)
2. **Chiang PH**, Wu PY, Kuo TW, Liu YC, Chan CF, Chien TC, Cheng JK, Huang YY, Chiu CD, Lien CC. (2012) GABA is depolarizing in hippocampal dentate granule cells of the adolescent and adult rats. *Journal of Neuroscience* 32:62-67. (Impact Factor: 6.7; Rank: Top 9.5% in Category of Neuroscience)
3. **Chiang PH**, Yeh WC, Lee CT, Weng JY, Huang YY, Lien CC. (2010) M₁-like muscarinic acetylcholine receptors regulate fast-spiking interneuron excitability in rat dentate gyrus. *Neuroscience* 169:39-51. (Impact Factor: 3.3)

HONOR & AWARDS

- ♦ Travel Awards from Foundation for the Advancement of Outstanding Scholarship to attend and present at Neuroscience 2014, Annual Meeting of Society for Neuroscience in Washington DC, USA (2014)
- ♦ Travel Awards from Foundation for the Advancement of Outstanding Scholarship to attend and present at Neuroscience 2011, Annual Meeting of Society for Neuroscience in Washington DC, USA (2011)
- ♦ Palm Scout Metal, the Top Achievement in Boy Scouting Program of Scouts of China (2002)

PROFESSIONAL MEMBERSHIP

- ♦ Member of the Society for Neuroscience (2010~Now)
- ♦ Member of Chinese Society of Cell and Molecular Biology (2013)

CONFERENCE PRESENTATIONS

1. **Chiang PH**, Chien TC, Chen CC, Lien CC. (2014) Characterization of acid-sensing ion channels in the mouse amygdala. Poster presentation, *Neuroscience 2014, Annual Meeting of Society for Neuroscience*
2. **Chiang PH**, Wu PY, Liu YC, Chien TC, Kuo TW, Cheng HJI, Lien CC. (2012) Excitatory actions of GABA in the dentate gyrus but not in the CA areas of the adult hippocampus. Poster presentation, *Neuroscience 2011, Annual Meeting of Society for Neuroscience*
3. **Chiang PH**, Yeh WC, Lien CC. (2010) M₁-like muscarinic acetylcholine receptors regulate fast-spiking interneuron excitability in rat dentate gyrus. Poster Presentation, *Neuroscience 2010, Annual Meeting of Society for Neuroscience*